Wood Joseph[1]

Three-phase catalytic reactors for hydrogenation and oxidation reactions

[1] School of Chemical Engineering, University of Birmingham, Edgbaston, Birmingham, B15 2TT, UK, E-mail: j.wood@bham.ac.uk

DOI: 10.1515/psr-2015-0019

Nomenclature

a	Exponent; Eq. (12)
a	Area; Eq. (36)
a_b	Gas-liquid interfacial area
A	Concentration of reactant A; Eqs. (18)–(23)
B	Concentration of reactant B; Eqs. (18)–(23)
b	Exponent; Eq. (12)
C_1	Constant; Eq. (12)
C	Constant; Eq. (13)
C_A^*	Equilibrium concentration of dissolved gas
Ca	Capillary number
C_{Ab}	Concentration of reactant A in the bulk
C_{Bb}	Concentration of reactant B in the bulk
C_{Ag}	Concentration of reactant A in the gas phase
C_{AS}	Concentration of reactant A at the catalyst surface
C_{H_2}	Concentration of hydrogen (dissolved)
C_i	Concentration of component i; Eqs. (22), (23)
C_j	Concentration of component j; Eqs. ((22), 23)
d	Impeller diameter
d_p	Particle diameter
d_{32}	Mean bubble size
D	Reactor diameter or diameter of capillary
$\mathscr{D}$	Diffusion coefficient; Eqs. (13), (38)
D_{AB}	Diffusivity of A through B
F_A	Molar flowrate of A
F_B	Molar flowrate of B
H	Henry's law constant
H	Liquid height in the reactor; Eq. (11)
k	Reaction rate constant; Eqs. (18)–(23)
k_i	Rate constant reaction i; Eq. (23)
$\underline{k}_1$	Pseudo first order rate constant
k_{cA}	Liquid-solid mass transfer coefficient
k_g	Gas-liquid mass transfer coefficient, gas side
k'_{gA}	Overall coefficient in trickle bed design; Eq. (26)
k_{lA}	Gas-liquid mass transfer coefficient, liquid side
$\overline{K}$	Consistency index; Eq. (13)
K_1, K_2, K_4	Adsorption coefficients of alcohol,oxygen and product; Eq. (16)
K_A	Adsorption coefficient of A; Eqs. (18)–(23)
K_B	Adsorption coefficient of B; Eqs. (18)–(23)
K_{H}	Adsorption coefficient of hydrogen; Eqs. (22), (23)
K_i	Adsorption coefficient component i; Eqs. (22), (23)
L	Length of liquid slug; Eq. (37)
m	Mass loading of catalyst in the reactor
n	Exponent; Eq. (13)

Wood Joseph is the corresponding author.

n_{cr}	Critical impeller speed
P	Power input per unit volume
P	Pressure; Eqs. (18)–(23)
P_H	Pressure of hydrogen; Eq. (22)
q	Volumetric gas flowrate
r_b	External resistance at the gas bubble
r_c	External resistance at the catalyst particle
r_r	Internal resistance at the catalyst particle
$-r_{AW}$	Actual observed rate per unit mass of catalyst
$-r^i_{AW}$	Intrinsic rate of reaction per unit mass of catalyst
R	Ideal gas constant; Eq. (22)
R'_A	Rate of reaction per unit bed volume
Re	Reynolds number
Sc	Schmidt number
Sh	Sherwood number
T	Temperature
U	Fluid velocity; Eq. (16)
U_g	Superficial gas velocity; Eq. (13)
U_t	Terminal velocity of a bubble in free rise; Eq. (13)
v_{sg}	Superficial gas velocity
V	Velocity
V_L	Liquid volume
W	Mass of catalyst
X_A	Conversion of A
Greek Letters	
α	Exponent
δ	Film thickness
ε	Voidage
ε_b	Bed density
$\bar{\varepsilon}_T$	Mean specific energy dissipation rate
η	Catalyst effectiveness factor
μ	Liquid viscosity
$\bar{\mu}_a$	Apparent viscosity of slurry in stirred tank
$\bar{\mu}_w$	Viscosity of slurry in water
ρ	Liquid density
$\bar{\rho}_l$	Apparent density of slurry; Eq. (13)
ρ_p	Particle density
σ	Liquid surface tension
ϕ	Thiele modulus
Additional Subscripts	
C	Capillary
G	Gas
L	Liquid
OV	Overall
S	Solid
$slug$	Slug
TP	Two phase

1 Introduction

The term "three phase catalytic reactors" generally refers to gas-liquid-solid reaction systems, in which the solid is typically a heterogeneous catalyst [1]. A fundamental division of three-phase reactors may be made by whether the solid phase is suspended in the liquid as in a slurry reactor, present as a fixed bed typical of a trickle bed reactor, or attached to some kind of structured support, for example a monolith reactor. Three-phase reactors have found extensive application in industry, for example in the production of bulk and fine chemicals, production of petroleum product and biochemical reactions. Winterbottom and King [2] have listed some typical applications of three-phase reactors as: triglyceride hydrogenation, hydrodesulphurization, hydrocracking, methanol synthesis and fine chemical synthesis. Examples of the latter include geraniol hydrogenation for the production of fragrances, conversion of nitriles to primary amines (for use in the production of pharmaceuticals), manufacture of dyestuffs, specialty chemical production, such as the alkylation of phenol, reaction of glucose to produce sorbitol. A number of textbooks have been devoted to the subject of multiphase catalytic reactors [3, 4]. However, the subject remains an active field of research for a number of reasons. These

include the development of new catalysts with enhanced selectivity and reaction rate, the emergence of a range of non-invasive imaging techniques that lead to new insights into reactor behavior and the new generation of reactor modeling capabilities such as computational fluid dynamics. Industrial drivers towards the study of three-phase reactors include a requirement to increase productivity and profit margins, maximize catalyst lifetime, as well as environmental considerations such as the reduction of waste and efficient use of raw materials. Emerging industries such as the conversion of biofeedstocks and utilization of heavy fossil fuels from the bottom of the oil barrel have also driven the need for new applications of three-phase reactors. The aim of this chapter is to provide a brief review of the theory of three-phase reactors, although more detailed texts are referred to for a thorough treatment, before reviewing a range of relevant research in the field of three-phase reactors. The chapter is divided according to slurry, trickle bed and structured catalysts.

2 Slurry Reactors

The slurry reactor may be defined as a three phase catalytic reactor in which the catalyst is in the form of small particles, which can be porous or non-porous, with a size typically in the range 50–200 μm or even less, where the fluid motion suspends the particles in the liquid [1]. Such reactors can be further sub-divided into stirred tank reactors, where fluid motion is induced by an impeller, or bubble column reactors, where the fluid motion occurs as a result of vigorous bubbling of gas through the liquid phase. Slurry type reactors are often operated as semi-batch or batch reactors, which offer good flexibility for processes such as fine chemicals and pharmaceuticals, where product recipes may regularly change and batch traceability is required. The process engineering must be considered when selecting a suitable type of reactor, for example the slurry reactor requires the catalyst to be separated after reaction, representing an additional cost of filtration. Slurry reactors are attractive for highly exothermic reactions because of their high liquid holdup/catalyst mass. Bubbling slurry reactors are useful for processes such as fermentation, which are catalyzed by biocatalysts.

2.1 Theory: Determination of Controlling Resistance

Although slurry reactors have been an industry workhorse for many years, their design is complicated due to the interplay between physical processes such as mixing, diffusion and mass transfer with chemical reaction processes. Therefore, gas-liquid and liquid-solid mass transfer, pore diffusion and suitable reaction kinetic models must be taken into consideration. The analysis of such reactors typically follows the reaction of a gas (A) with liquid reactant (B) to produce a liquid phase product (P). A number of steps occur in the course of this process, which include:

1. Absorption of A from the gas phase in to the liquid;
2. Diffusion of A across a boundary layer at the gas-liquid interface;
3. Diffusion of A through the bulk liquid;
4. Diffusion of A across a boundary at the external surface of the catalyst particle;
5. Internal diffusion of A and B through the catalyst pores;
6. Reaction of A and B at the active sites of the porous catalyst;
7. Diffusion of products out of the catalyst pellet.

Figure 1 depicts the various mass transfer and reaction steps that must take place in order for the reactants to reach the catalyst surface and react, together with the relevant interface concentrations of A. The equations associated with each step are outlined in Table 1. The reader is referred to Winterbottom and King [2] or Fogler [5] for a full derivation of the relevant equations. These simple models are useful in understanding the parameters that control the three-phase reactor and hence how the design may be optimized to achieve the maximum reaction rate, as briefly discussed below.

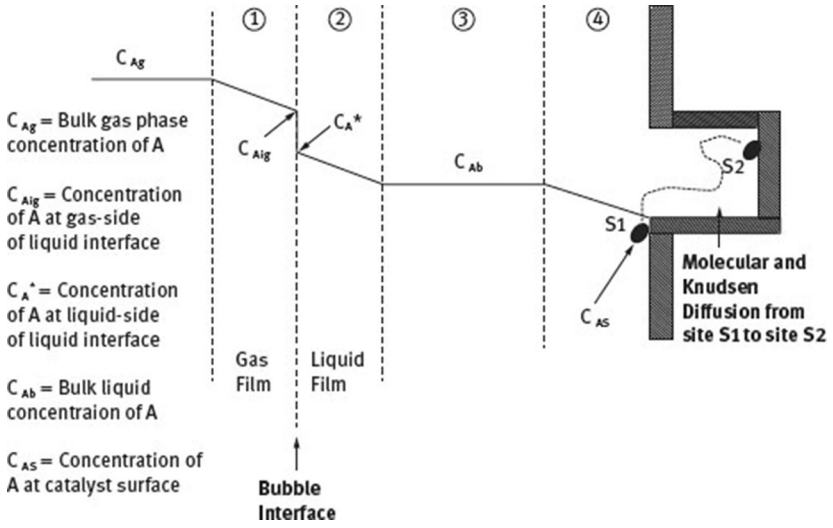

Figure 1: Resistances at the gas-liquid and liquid-catalyst interfaces in a three-phase reactor system.

Table 1 Summary of expressions for mass transfer, diffusion and reaction parameters in the three-phase catalytic reactor, following analysis of Winterbottom and King [2].

Process	Expression	Eq.
Dissolution of gas at the gas-liquid interface, according to Henry's law	$C_A^* = \frac{C_{Aig}}{H}$	(1)
Rate of mass transfer from gas-liquid interface to bulk liquid	$R_A = k_{lA}\, a_b\, (C_A^* - C_{Ab})$	(2)
Rate of mass transfer across boundary layer at external surface of catalyst pellets	$R_A = k_{cA}\, a_c m\, (C_{Ab} - C_{AS})$	(3)
Rate of diffusion and reaction in the catalyst pores	$R_A = m\, (-r_{AW})$	(4)
Relation of actual reaction rate to intrinsic rate	$R_A = m\eta\, (-r^l_{AW})$	(5)
Expression for catalyst effectiveness factor for first order reaction in a spherical catalyst pellet	$\eta = \frac{3}{\phi}\left[\frac{1}{\tanh\,\phi} - \frac{1}{\phi}\right]$	(6)
Thiele modulus	$\phi = \frac{d_p}{2}\sqrt{\frac{\rho p \underline{k}_1}{D_{\text{eff}}}}$	(7)
Pseudo first order reaction rate in hydrogen	$(-r^l_{AW}) = \underline{k}_1 C_{AS}$	(8)

Overall slurry reactor model

$$\frac{C_A^*}{R_A} = \frac{1}{k_{lA}a_b} + \frac{1}{m}\left(\frac{1}{k_{cA}a_c} + \frac{1}{\eta k_1}\right) \quad (9)$$

or

$$\frac{C_A^*}{R_A} = r_b + \frac{1}{m}(r_c + r_r) \quad (10)$$

Gas absorption

It is observed from Eq. (1) of Table 1 that the concentration of dissolved gas at the interface is dependent upon Henry's law, where Henry's law constant (H) is a measure of the solubility of gas in the particular solvent or reactant used and varies as a function of reactor operating temperature. Here it is assumed that concentration gradients in the gas phase are negligible, if the gas bubbles contain only small amounts of components other than A, or if A is only sparingly soluble in the liquid phase.

Diffusion processes

Eqs. (2) and (3) represent the respective gas-liquid and liquid-solid mass transfer steps, encompassing the mass transfer coefficients for the gas-liquid (k_{lA}) and liquid-solid (k_{cA}), the gas-liquid interfacial area (a_b), catalyst specific surface area (a_c) and mass loading of catalyst in the reactor (m).

Reaction in the catalyst particle

Eqs. (4)–(8) represent the diffusion/reaction processes, the actual observed rate ($-rAW$) expressed in Eq. (4) with the intrinsic rate that would occur over a finely crushed catalyst without diffusion limitations ($-r^I_{AW}$) and the catalyst effectiveness factor (η) being expressed in Eq. (5). In Eq. (8), it is assumed that the liquid phase reactant is present at a sufficiently high concentration that the kinetics become first order in terms of hydrogen concentration at the catalyst surface (C_{AS}) with pseudo first order rate constant.

Overall slurry reactor model

Eq. (9) represents a combination and rearrangement of Eqs. (1)–(5) and (8) to provide an overall slurry reactor model, where r_b is a mass transfer resistance at the gas bubble, r_c is a mass transfer resistance at the external surface of the catalyst particle and r_r represents internal diffusion/reaction resistance inside the catalyst particle. The slurry reactor 'model' can be expressed as a graphical plot of C_A^*/R_A against reciprocal catalyst loading ($1/m$), as shown in Figure 2. Thus the slope of the graph represents the combined external diffusion resistance r_c and internal diffusion/reaction resistance r_r at the catalyst particle, whilst the intercept of the graph represents the gas absorption resistance at the gas-liquid interface, r_b. The intercept in Figure 2 is determined only by the gas absorption resistance, which could be altered by the use of an improved sparger design or higher gas pressure. The slope of the graph, representing the resistances at the catalyst particle is influenced by the catalyst particle size, and therefore internal and external diffusion resistances can be decreased by using a more finely crushed catalyst particle.

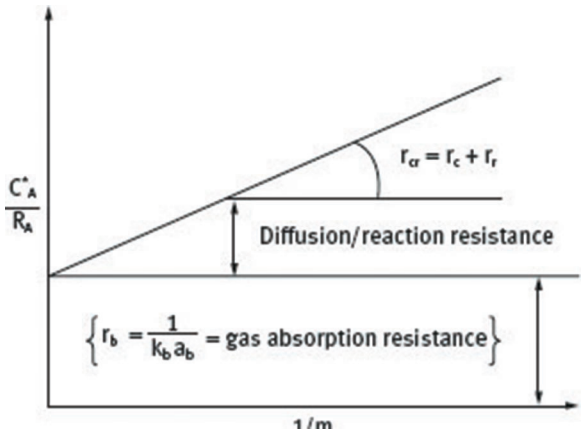

Figure 2: Plot of equilibrium dissolved gas concentration/reaction rate versus reciprocal catalyst loading, showing magnitude of resistances at the gas-liquid interface and catalyst particle.

2.2 Mixing and mass transfer in the stirred tank slurry reactor

The introductory sections of this chapter showed that the slurry reactor performance may be influenced by both reaction kinetics and various mass transfer resistances, associated with gas absorption and diffusion at the catalyst particle. In order to design or predict the performance of the stirred tank reactor, the gas-liquid and liquid-solid mass transfer coefficients must be calculated. Markopoulos *et al*. [6] has reviewed mass transfer coefficients in mechanically agitated gas-liquid contactors. There are many correlations reported for the prediction of gas-liquid (liquid-side) mass transfer coefficients in stirred vessels, such that no single correlation is suitable for all situations. Rather the type of fluid (Newtonian or non-Newtonian), geometry of the system and type of impeller must be considered in selecting a suitable correlation. For low-viscous and coalescing Newtonian fluids a number of correlations have been proposed in the literature, which are dependent upon material properties, geometry of the system and operating conditions, of the form:

$$k_l a = f\left(P/V_L, v_{sg}, H/D, d/D, q/V_L, \rho, \mu, \sigma\right) d, \tag{11}$$

where k_{la} is the volume based liquid side mass transfer coefficient, P/VL is the power input, P is per unit liquid volume, VL, v_{sg} is the superficial gas velocity, H is the liquid height in the reactor, d/D is the ratio of the impeller diameter to the reactor diameter, q/VL is the volumetric gas flow rate, q, per unit liquid volume, ρ is the liquid density, μ is the liquid viscosity and σ is the liquid surface tension. For a given geometry, a critical impeller speed exists, n_{cr}. For impeller speed $n < n_{cr}$, the interfacial area and volume-related mass transfer coefficient depends on the gas load and not on the speed of the agitator. For $n > \mathrm{n_{cr}}$, the volume-related mass transfer coefficient increases linearly with impeller speed. In this region, there is no effect of the gas flow rate on a and k_{la}. Figure 3 shows a cut-away diagram of the stirred tank reactor. Various types of impellers are available, including pitched blade turbines and Rushton turbines, as shown in Figure 4. For given geometry and fluid properties, the mass transfer coefficient is often expressed as:

$$k_l a = C_1 (P/V_L)^{a_1} v_{sg}^{b1}. \tag{12}$$

The exponents, a and b vary for different systems, depending upon the stirrer and gas distributor designs, whilst the constant C is influenced by the liquid type and properties. Three phase slurry reactors contain a dispersion of solid catalyst particles, whilst many gas-liquid mass transfer correlations do not allow for the presence of the particles upon the mass transfer process. Kawase *et al*. [7] found that volumetric mass transfer coefficients in water decreased due to the presence of solid particles at constant impeller speed and superficial gas velocity, and proposed an extended mass transfer correlation for gas-liquid-solid three-phase systems:

$$k_l a = C' \sqrt{(\mathscr{D})} \frac{\rho_l^{-3/5} \varepsilon^{(9+4n)/10(1+n)}}{\left(\bar{K}/\bar{\rho}_l\right)^{1/2(1+n)} \sigma^{3/5}} \left(\frac{U_g}{U_t}\right)^{1/2} \left(\frac{\bar{\mu}_a}{\bar{\mu}_w}\right)^{-0.25} \tag{13}$$

Where C' is a constant, D is diffusivity, $\bar{\rho}_l$ is apparent density of slurry, $\overline{K}$ is a consistency index of slurry, σ is surface tension, U_g is superficial gas velocity, U_t is terminal velocity of a bubble in free rise, $\bar{\mu}_a$ is apparent viscosity of slurry in stirred tank and $\bar{\mu}_w$ is viscosity of slurry in water.

Hydrogenation reactions are an important class of industrial reaction, which may be strongly influenced by gas-liquid mass transfer considerations. They are often carried out in a solvent in order to dissolve the reactant, to absorb heat of reaction and to solubilize coke precursors from the catalyst surface. In recent years, there has been a motivation to use 'greener' solvents rather than volatile organic carbons (VOCs) for environmental considerations, for example water or supercritical carbon dioxide. It has also been shown that the type of solvent used can influence the rate and selectivity of the reaction. A number of reasons have been suggested to explain the solvent effects observed [8]:

1. The solubility of hydrogen in the reaction media;
2. Competitive adsorption of solvent at active catalyst sites;
3. Agglomeration of catalyst in some solvents;
4. Intermolecular interaction between the reactant and solvent molecules.

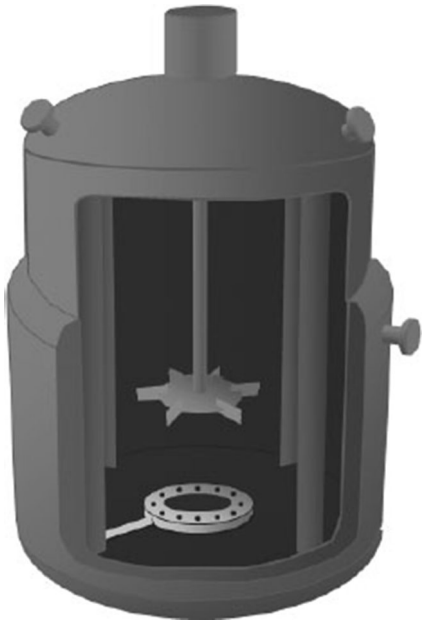

Figure 3: Schematic of a stirred tank reactor with Rushton turbine and gas sparger.

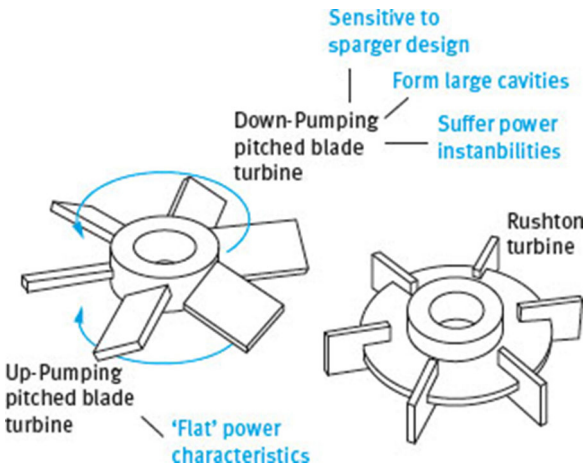

Figure 4: Pitched blade and Rushton turbines and their characteristics.

The reaction rate in a particular system may have a complex dependence upon the system properties, including the selection of solvent [9]. In addition to the solvent effects listed above, under typical industrial conditions the reaction rate may be mass transfer controlled and thus dependent on the gas-liquid interfacial area. Hu *et al.* [9] studied the effect of solvent composition, including water, 2-propanol and mixtures of the two upon three-phase hydrogenation of 2-butyne-1,4-diol on Pd/Al_2O_3 catalysts in a stirred reactor with mean specific energy dissipation rates, $\bar{\varepsilon}_T$, up to 50 W kg^1. The investigations were carried out using a 3 l reactor operated at 1 barg pressure, 35 °C and with a 12 % v/v headspace prior to sparging. Pd/Al_2O_3 particles and alumina particles

were mixed to give an overall metal content of 1 wt % Pd whilst reducing the number of dark Pd particles to improve the observation of bubbles. For the first time, bubble sizes were measured *in situ* with reaction rates using a video-microscope-computer system [10] during reaction via a viewing window protruding very slightly in to the vessel, at a constant flow rate of 0.25l/min hydrogen at 1 barg. Typical bubble images are shown in Figure 5. The stirred tank was agitated using an up-pumping pitch blade turbine for the two-step hydrogenations, whilst the second step of 2-butene-1,4-diol to the alkane used a Rushton turbine.

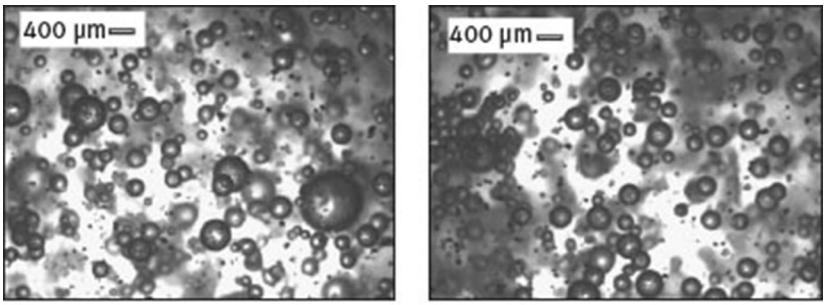

Figure 5: Bubble images at $\bar{\varepsilon}_T = 3.3\,\mathrm{W/kg}$ during hydrogenation of 2-butene-1,4-diol in water: (a) 20 min after beginning the reaction; (b) post-reaction. Reprinted from Hu *et al*. © [9], with permission from Elsevier.

The hydrogenation of alkynes is often studied as a model for the investigation of three-phase reactions. The reaction scheme is shown in Figure 6. The desirable product in alkyne hydrogenations is often the cis-alkene, where 2-butene-1,4-diol is used in the manufacture of products such as vitamins and insecticide, the over hydrogenation to the alkane or formation of side products being undesirable. Hu *et al*. [11] also reported bubble size measurements for air-water systems; they indicated that in the single component solvents, irregular, relatively large bubbles with a wide size distribution were observed. In the mixed aqueous/organic solvents, and especially at lower concentrations of IPA (1%, 5%, 10% v/v), the bubbles were spherical, much smaller and with a narrow size distribution. This was explained as being due to interaction between the organic and aqueous phase leading to lower incidence of coalescence in mixed solvents. A similar effect was observed during and after the reaction in the hydrogenation of 2-butyne-1,4-diol, as shown by the Sauter mean bubble size, d_{32}, versus solvent concentration in Figure 7 [9]. The bubble size is observed to pass through a minimum at a concentration of 5% v/v 2-propanol in water. Figure 8 shows the average uptake of hydrogen for the two-step reaction as a function of solvent concentration. For both steps of the reaction, there is a peak at around 5 % v/v 2-propanol, followed by a fall to 30 % v/v before rising steadily to pure 2-propanol, where a rate approximately double that observed in water is achieved, although the solubility of hydrogen in 2-propanol is around six times higher than in water. The first step of the reaction was found to be under kinetic control, but the second step was determined to be under gas-liquid mass transfer control. The peaks in reaction rate observed in Figure 8 could be explained in terms of the bubble size and solubility of hydrogen. At a solvent concentration of 5 % v/v the smallest bubble size led to the highest interfacial area available to mass transfer of gas to liquid, and thus giving a peak in reaction rate at the corresponding concentration. As the amount of 2-propanol in the solvent mixture increased, the reaction rate initially decreased due to a larger bubble size and lower interfacial area. However, at the highest concentrations of 2-propanol it increased further due to the higher solubility of hydrogen in the organic solvent compared with water. This trend for reaction rate as a function of solvent composition was predicted by the parameters bubble size and hydrogen solubility. When the reaction is under gas-liquid mass transfer control, the overall rate can be expressed by the proportional relationship:

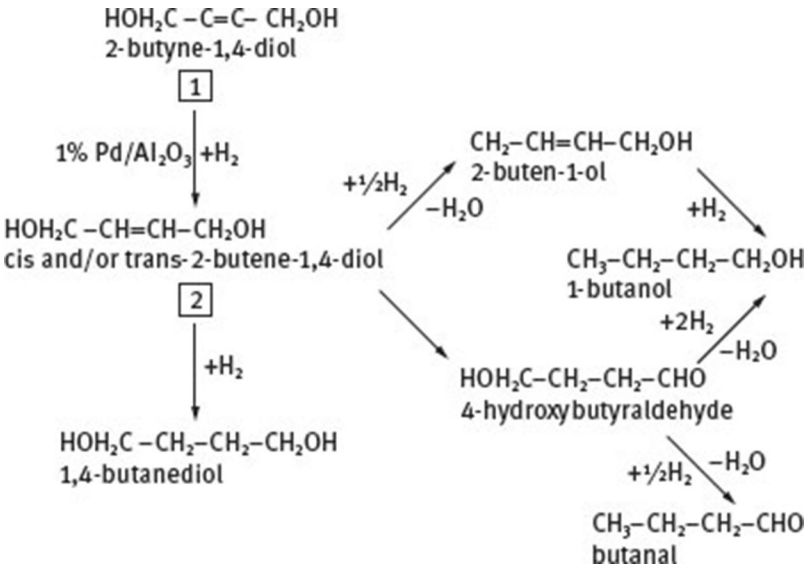

Figure 6: Reaction scheme for the hydrogenation of 2-butyne-1,4-diol. Reprinted from Hu *et al*. © [9], with permission from Elsevier.

$$r \alpha C_{H_2}/d_{32}. \tag{14}$$

Liquid-solid mass transfer resistance at the outside surface of the catalyst particle may be a significant consideration for large particles or slowly agitated systems. If shear stress occurs between the particle and fluid, an appropriate form of the Frössling equation may be used to calculate the liquid-solid mass transfer coefficient:

$$Sh = 2.0 + 0.6\,\mathrm{Re}^{1/2}\,Sc^{1/3}, \tag{15}$$

where Sh is the Sherwood number,$Sh = \frac{k_{cA} d_p}{D_{AB}}$. At sufficiently high shear stresses such that the Reynolds number has the dominant effect upon the Sherwood number, it is found that the mass transfer coefficient is mainly influenced by fluid velocity and particle diameter, according to the relationship

$$k_{cA}\,\alpha\,\frac{U^{1/2}}{d_p^{1/2}}. \tag{16}$$

Thus increasing the fluid velocity, U, or using a smaller catalyst particle diameter, d_p, can be used to increase the liquid-solid mass transfer coefficient.

Fishwick *et al*. [12] asserted that the design of stirred vessels has been more of an art than science, relying on "black box" type approaches. Poorly understood mixing issues may lead to the loss of several billion dollars per year to the related process industries. However, this approach is starting to change owing to various non-invasive imaging techniques such as Electrical Capacitance Tomography (ECT), Positron Emission Particle Tracking (PEPT) and Particle Image Velocimetry (PIV). Such techniques can be used to obtain information such as fluid trajectories, velocity distributions, velocity gradients and shear rates. The design of stirred reactors presents a challenge in order to achieve bulk fluid motion to guarantee good circulation in the mixing vessel, whilst also achieving suspension of the catalyst particles and dissipation of the gas bubbles throughout the fluid, requiring adequate local velocities to be achieved in the parts of the vessel remote from the impeller. The majority of earlier two-phase studies investigated the velocity fields occurring with Rushton turbines, using Laser Doppler Velocimetry (LDV) [13] or PIV [14]. However, such optical techniques have mainly been carried out at low gassing rates and without particles, since once the fluid in the vessel becomes opaque due to gas and particle dispersion, such optical techniques cannot be used. Radioactive particle tracking techniques developed at Washington University (Computer Automated Radioactive Particle Tracking CARPT [15]) and at the University of Birmingham (Positron Emission Particle Tracking, PEPT [16]) provided the advantage of being able to study fluid trajectories in opaque systems. Also, because the tracked particle is carried with the flow field, Lagrangian data are collected. In the study of Fishwick *et al*. [17] the liquid phase mixing in gassed vessels agitated by up-and downward pumping 30° and 45° pitched-blade turbines was investigated using PEPT. The PEPT technique uses a radioisotope that decays by β^+ decay, which involves the emission of a positron. The

emitted positron is annihilated by an electron, leading to the release of energy in the form of two back-to-back gamma rays, as shown in Figure 9. The γ-rays are detected with two γ-ray cameras positioned either side of the vessel and their paths are reconstructed. From several such events the location of the tracer can be determined. A computer algorithm removes erroneous detections, allowing the tracer to be tracked within the vessel ~ 250 times per second within to 0.5 mm at the time of the experiment in 2007. A neutrally buoyant tracer was used based on an anion exchange resin labeled with ^{18}F.

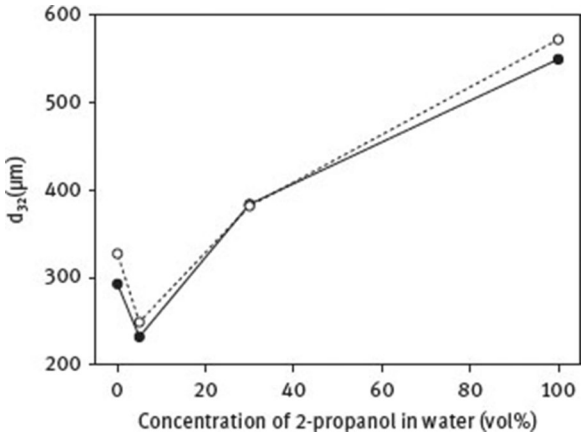

Figure 7: Bubble diameter, d_{32}, versus concentration of 2-propanol in water during (○) and post reaction (●). Reprinted from Hu *et al*. © [9], with permission from Elsevier.

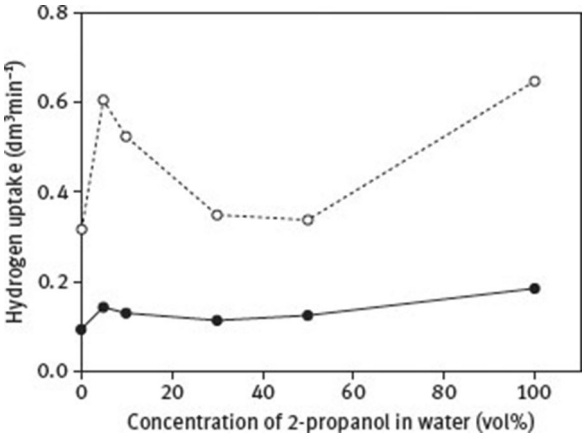

Figure 8: Reaction rate versus concentration of 2-propanol in water for hydrogenation of 0.2 M 2-butyne-1,4-diol:● first step; ○ second step. Reprinted from Hu *et al*. © [9], with permission from Elsevier.

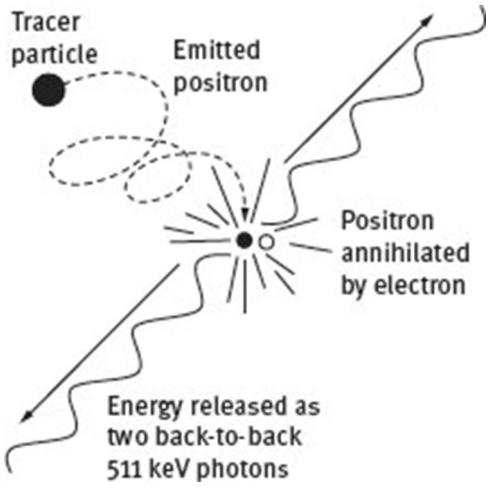

Figure 9: Formation of back-to-back γ-rays from an emitted positron. From several such events, the tracer can be located by triangulation. Reprinted from Fish-wick *et al*. © [12], with permission from American Chemical Society.

The effect of gassing on mean liquid velocity fields is shown in Figure 10, for four impellers. In Figure 10 (a) i the flow pattern is typical for down-pumping pitched blade turbines, with the discharge at ~ 45° to the

vertical. A primary circulation loop is formed in the lower part of the vessel, with a weak secondary circulation loop in the upper part, circulating clockwise. Below the impeller the liquid circulates upward into the impeller to form another loop. Figure 10 (a) (ii) shows the effect of gassing on the system, whereby the injection of gas at a specific flowrate of 1.5 vvm was studied. After the introduction of gas the flow field changed considerably, and the impeller discharge became essentially radial, suggesting that the effect of gassing had a more dominant effect than the impeller. In Figure 10 (b), the effect of gas introduction had a weaker effect upon the flow pattern for the 30° PBTD. Figure 10 (c) (i) presents the flow patterns for the 45° PBTU, showing a strong circulation loop in the flower part of the vessel near the impeller discharge. In the upper part of the vessel, a weaker secondary circulation loop was induced. The addition of gas was found to destabilize this loop and the upward flow of gas at the wall forced the eye of the secondary loop slightly inward towards the center of the vessel (Figure 10 (c) (ii)). Similar results were obtained with the 30° PBTU (Figure 10 (d) (i) and (ii)). In order to further interpret the data, a fluid circulation index was defined as the ratio of the average particle circulation velocity to the impeller tip speed:

$$I_c = \frac{v_m}{v_{tip}}. \tag{17}$$

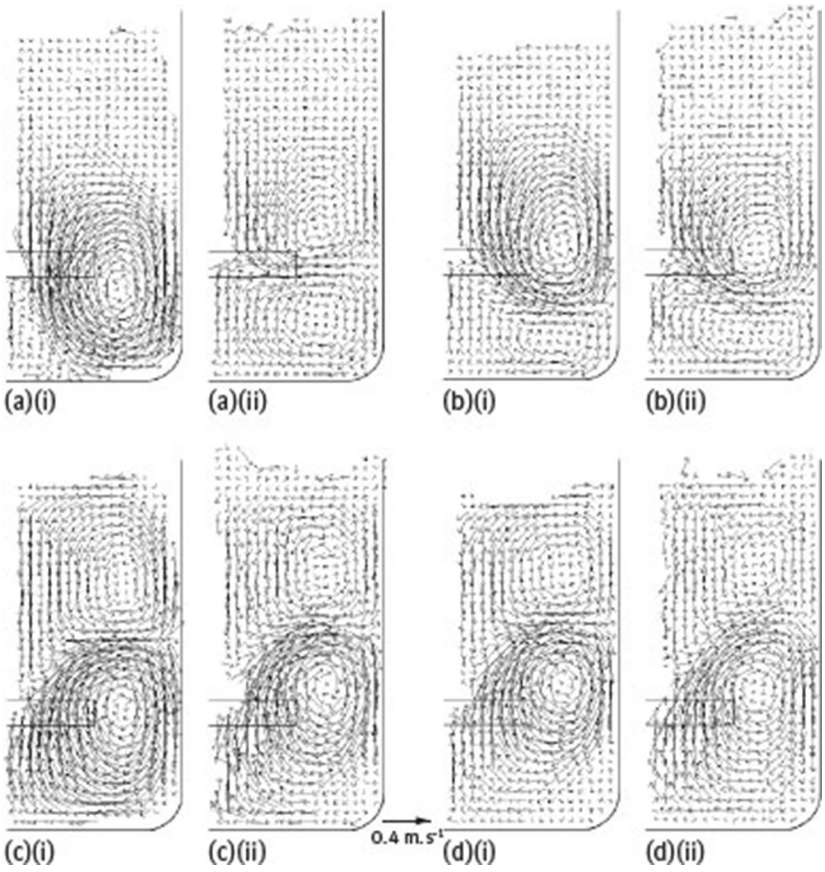

Figure 10: Mean radial-axial velocity vector plots for (a) a 45° PBTD, (b) a 30° PBTD, (c) a 45° PBTU, and (d) a 30° PBTU ((i) without gassing and (ii)with a specific gas flow rate of 1.5 vvm) as measured using PEPT. Reprinted from Fishwick *et al*. © [12], with permission from American Chemical Society.

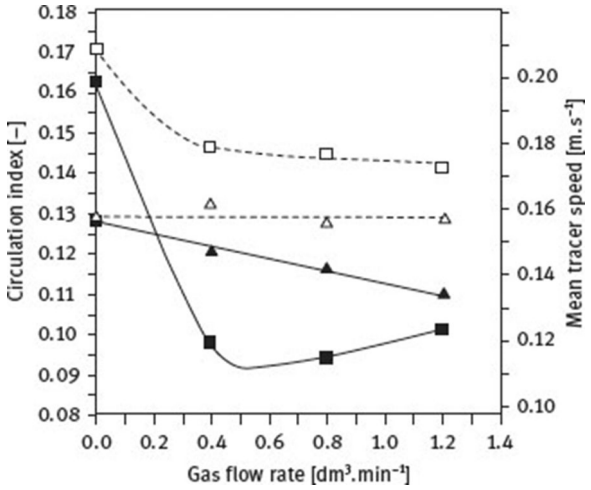

Figure 11: Circulation index (mean tracer speed/impeller tip speed) at different volumetric gas flow rates at $N = 483$ min^{-1} for (▪) 45° PBTD, ( ) 30° PBTD, ( ) 45° PBTU, and (( ) 30° PBTU. Reprinted from Fishwick *et al*. © [12], with permission from American Chemical Society.

Figure 11 shows the circulation index for the four impellers as a function of the gas flow rate. The effect of gas flow rate has only a negligible effect upon the circulation index for the 30° PBTU, whilst the 30° PBTD showed only a slight decrease of circulation index with increased gassing. The 45° PBTU showed an initial decrease in circulation index with initial gassing, but this leveled out at gas flows above 0.4 dm^3 min^{-1}. The most dramatic effect was observed upon the 45° PBTU, which showed a significant decrease of ~ 38 % with the injection of gas over the range of gas flow rates studied, indicating decreased momentum transfer capacity, being the poorest of the impellers studied in the gassed system. Electrical Resistance Tomography presents an alternative technique for the study of gassing of mixing vessels, which can be applied to plant scale systems [18]. The goal of electrical resistance tomography is to obtain the resistance distribution in the domain of interest. It can be obtained in a particular cross section by injecting currents on the domain and measuring voltages on it via a number of spaced electrodes, which are mounted non-invasively on its boundary. UMIST developed the necessary sensor, data acquisition and reconstruction systems, incorporating and 8-plane 16-electrode ring sensor which were applied to measurements on a 1.5 m-diameter pilot plant stirred tank. The system was used to study the impact of stirring on gas-liquid mixing with a Rushton turbine. The impeller created a strong radial outflow, giving a lower gas hold-up in the impeller plane. The gas hold-up immediately below the impeller was higher and there was also a higher gas hold-up in the liquid being drawn back towards the agitator in the upper part of the vessel. Some asymmetry in the gas hold-up was observed, resulting from the baffles of the tank disrupting the tangential flow. The measurements were used to validate networks of zone models of stirred tank mixing.

2.3 Hydrogenation reactions in the stirred tank slurry reactor: kinetics and effect of operating variables

The slurry reactor is often used for carrying out hydrogenation reactions, particularly for the case of fine chemicals and pharmaceuticals, where changes to product requirements and batch traceability are required. Mills and Chaudhari [19] reviewed the use of multiphase reactors in the pharmaceuticals and fine chemical production, wherein for gas-liquid-solid systems the reaction essentially occurs at the catalyst surface. These reaction mechanisms are often described using classical Langmuir-Hinshelwood reaction models. Such models consider the various reversible adsorption, formation of intermediates, reaction and desorption steps that could occur in the course of the reaction, together with the surface fractional coverage of the catalyst surface with each component. The rate-determining step is used in order to derive the overall reaction rate, as outlined by Froment [20]. Mills and Chaudhari [19] summarized some examples of kinetic rate equation models for gas-liquid-solid catalytic reactions that are relevant to fine chemicals and pharmaceuticals, a selection of which are given in Table 2.

Table 2 Kinetic expressions for some typical hydrogenation reactions. Adapted from Mills *et al*. [21], with permission of Elsevier.

Reaction System	Catalyst	Kinetic Model	Eq.

Hydrogenation of glucose [22]	Raney-Ni	$\frac{Wk_{11}AB}{(1+K_AA)}$	(18)
Hydrogenation of *o*-nitroanisole [23].	Pd/C	$\frac{WkAB}{(1+K_AA)(1+K_BB)}$	(19)
Hydrogenation of 2-ethylhexenal [24].	Pd-SiO_2-monolithic	$\frac{WkAB}{\left(1+\sqrt{K_AA}+K_BB+K_PP\right)^3}$	(20)
Hydrogenation of *m*-nitrochlorobenzene [25].	Pt-S/C	$\frac{WkAB}{(1+K_BB)}$	(21)
Hydrogenation of 2,4-dinitrotoluene [152].	Pd/Al_2O_3	$r_i = \frac{kK_HK_i(P_H/RT)^{0.5}C_i}{\left[1+K_H(P/RT)^{0.5}\right]\left[1+K_iC_i+\sum_{ji}K_jC_j\right]}$	(22)
Hydrogenation of 1,5,9-cyclododecatriene [153].	Pd/Al_2O_3	$r_i = \frac{Wk_iK_jA^\alpha C_j}{\left(1+\sum_{j=1}^{3}K_jC_j\right)}$	(23)

The expressions listed in Table 2 represent intrinsic kinetics; any associated mass transfer resistances also need to be evaluated in order to determine the actual rate of reactions. For reactions involving dissolved gas and liquid phase reactants and products, the complications of competitive adsorption, solvent effects and solubility of the reacting gas in the solvent should also be considered. In applications where more than one elementary step can be rate limiting, the equations in Table 2 are not valid and the development of a suitable kinetic model becomes a challenge.

The early understanding of the mechanisms and kinetics of hydrogenation of alkynes and alkenes was largely contributed by research in the 1960s by Bond and Wells [26, 27] and Feidlin and Kaup [28], particularly in the case of ethyne and ethene. The hydrogenation of ethyne on Pd/Al_2O_3 catalysts is a well-studied gas-solid reaction of industrial importance, as it is used for the removal of ethyne impurities from ethane prior to polymerization. The understanding of selectivity issues in ethyne hydrogenation requires an understanding of the adsorption models of ethyne and ethane upon the catalyst. Arafa and Webb [29] suggested that three types of active sites exist on the catalyst surface, including Type I sites which are active for ethyne hydrogenation to ethane; Type II sites which are active for direct hydrogenation of ethyne to ethane and Type III sites that are active for hydrogenation of ethane to ethane. A number of studies reported mechanisms of the reaction, incorporating different hydrogenation and oligomerization routes [30, 31]. Borodzinski and Cybulski [32] reported a model for ethyne hydrogenation that allowed for the reaction over a surface on which some carbonaceous deposits already exist. They assumed that there are three types of active sites, created on the palladium surface by carbonaceous deposits. Their model was novel in the consideration of the role in the kinetic analysis of (1) carbonaceous deposits creating a heterogeneous surface and (2) the transfer of hydrogen atoms from the carbon to hydrogenate ethyne. During ethyne hydrogenation a number of surface polymers may be formed [33], as well as butane and benzene [34, 35]. A known side product of ethyne hydrogenation is green oil, which is comprised of alkanes and alkenes of high molecular weight. The green oil can poison or block access to the ethyne hydrogenation sites of the catalyst. In more recent times, researchers have sought to understand whether the same effects occur in the hydrogenation of higher hydrocarbons [36].

Palladium is a highly selective catalyst for the hydrogenation of unsaturated hydrocarbons, offering high selectivity in alkyne over alkene hydrogenation and preferential cis/trans ratio of alkene products [37]. The hydrogenation of 1-pentyne and 2-pentyne over three different types of palladium catalysts was studied by Jackson *et al*. [36]. It was found that the internal triple bond hydrogenated faster than the terminal bond over a Pd/C catalyst. A support particle size effect was suggested. Boitiaux *et al*. [38] studied the effect of metal particle size and dispersion, and found that increasing metal dispersion above 20 % led to a reduction in the

activity of but-1-yne hydrogenation. This resulted from a stronger complexation of alkyne to the metal over smaller particles, which tend to be electron deficient. Boitiaux *et al*. [39] reported increased activity of supported palladium catalysts upon the addition of an electron-donating additive, such as piperidine in the hydrogenation of 1-butyne. The additive was proposed to modify the complexation strength of the alkyne with the metal, similar to the effect of a ligand in homogeneous catalysis. Increased alkene selectivity was observed as the rate of alkyne hydrogenation accelerated, but alkene hydrogenation decelerated.

Competitive effects may occur in hydrogenation of multiple alkyne substrates, as investigated by Hamilton *et al*. [40] over a Pd/C catalyst. The reaction of pairs of 1-pentyne, phenyl acetylene, 2-pentyne and 1-phenyl-1-propene were studied and it was revealed that a lower hydrogenation rate typically occurred for both alkynes compared to either single reactant. However, a rate enhancement was observed for the 1-pentyne/2-pentyne system, which was through to be a result of enhanced hydrogen transfer on the surface.

The hydrogenation of 1-pentyne over a range of palladium catalysts was studied by Teschner *et al*. [41], applying techniques such as catalytic pulse experiments, tapered element oscillating microbalance and catalytic pulse experiments. A carbonaceous Pd-C surface phase was found to build up in the early stages of the reaction, upon which the reaction subsequently occurred. Similar observations were made in the hydrogenation of C_2 alkynes, where the reaction is well known to occur upon a layer of surface deposited carbon [26, 27].

Competitive effects were also studied in the hydrogenation of 1-pentene, cis-2-pentene and trans-2-pentene over a 1 % Pd/alumina catalyst by Canning *et al*. [42]. Cis-2-pentene hydrogenated faster than 1-pentene, which in turn was faster than trans-2-pentene. The rate of 1-pentene hydrogenation was greatly accelerated by 20-fold in a competitive system between alkene and alkyne, even after complete consumption of alkyne. Enhanced hydrogen transfer was believed to occur through a modified layer of hydrocarbon deposits upon the catalyst surface.

Bennett *et al*. [43] studied the hydrogenation of 2-pentyne over Pd/Al_2O_3 catalysts, with a view to understanding scale up and effect of operating variables in the stirred tank reactor. The research was also intended to contribute towards gaps in knowledge of the hydrogenation mechanisms and reactivity for > C_4 alkynes in the liquid phase. The reactions were carried out in a 2.65 l baffled stirred vessel, using 1 wt % Pd/Al_2O_3 catalyst. The effects upon rate and selectivity of stirring speed, catalyst loading, substrate concentration, hydrogen pressure, solvent type and catalyst preparation method were investigated. Increasing the stirring speed from 445 rpm to 1100 rpm was found to lead to a substantial increase in reaction rate from 2.49×10^6 mol dm^{-3} s^{-1} to 4.38 mol dm^{-3} s^{-1}. The effect of stirring speed upon gas-liquid mass transfer was investigated by calculating the value of k_{la} from the correlation of Kawase *et al*. [7] (Eq. (13)) and liquid-solid mass transfer coefficient was calculated from the Frössling equation. It was found that the gas-liquid mass transfer coefficient k_{la} increased from a value of 7.93×10^{-4} to 4.63×10^{-3} s^{-1}, by a factor of 5.8 upon increasing the stirring speed, whereas the solid-liquid mass transfer coefficient, k_c, increased from 4.89×10^{-4} to 9.04×10^{-4} m s^{-1}, by a factor of 1.84. Calculation of the rates of hydrogen mass transfer indicated that the rate based upon liquid-solid mass transfer was close (within 12 %) to the observed reaction rate; therefore, it was assumed that the reaction was under external mass transfer control at the catalyst particle.

Owing to the likeliness of external diffusion control, Bennett *et al*. [43] found that using a reduced size of the catalyst support particle gave improved reaction rate. Particles with diameter in the range 45–75 μm rather than ~ 100 μm led to a substantial increase in reaction rate at a stirring speed of 1100 rpm, by a factor of ~ 10.3. The increase of reaction rate was greater than would be expected from the increase in liquid-solid mass transfer alone, although it should be noted that, with a given amount of catalyst, using particles of smaller size also gives a large surface area and thus the value of the specific surface area of the catalyst, a_c, also increases. The combined effect of liquid-solid mass transfer coefficient and increased surface area of particles could explain the observed increase in reaction rate.

Pre-treatment of a catalyst by reduction in hydrogen is commonly used to activate the catalyst by converting the catalytic metals from the oxide to metallic form. However, Bennett *et al*. [43] studied the effect of pre-treatment with hydrogen upon the product profiles during the hydrogenation reaction of 2-pentyne. It was found that when the catalyst is not pre-reduced prior to the addition of the reagents, the selectivity of the reaction is altered significantly. The rates of alkyne consumption and pentane formation are similar to those found over the pre-reduced catalyst, but the trans-alkene is formed to a much greater extent when the catalyst is not pre-reduced. This effect was explained, since when the catalyst is pre-reduced under hydrogen, the plentiful availability of hydrogen chemisorbed on the catalyst surface leads to the main reaction being hydrogenation to form cis-2-pentene. When the catalyst is not pre-reduced and has a lower coverage of hydrogen, isomerization reactions are favored over hydrogenations, and the observed production of trans-2-pentene increases. On the pre-reduced catalyst, the reaction is thought to involve the formation of a carbonaceous overlayer; but when the catalyst is not pre-reduced, the surface consists of Pd metal or oxide.

2.4 Catalysts for hydrogenation reactions: overview and novel biomass supported metal catalysts

A variety of catalyst preparation techniques are available, depending upon the required properties of the finished catalyst. The properties of the heterogeneous catalyst are influenced strongly by each step of the preparation method and the quality of the raw materials. Perego and Villa [44] have summarized the unit operations involved in catalyst preparation, as shown in Table 3.

Table 3 Typical steps involved in catalyst preparation. Reprinted from Perego and Villa © [44], with permission of Elsevier.

1.	Precipitation	7.	Calcination
2.	Gelation	8.	Forming operation
3.	Hydrothermal transformation	9.	Impregnation
4.	Decantation, filtration, centrifugation	10.	Crushing and grinding
5.	Washing	11.	Mixing
6.	Drying	12.	Activation

Most catalyst formulations comprise a combination of some or all of the above operations. Whilst methods of preparation vary widely, three broad classifications of catalyst can be made according to their preparation procedure, namely: (1) Bulk catalysts and supports; (2) Impregnated catalyst; and (3) Mixed-agglomerated catalysts. Bulk catalysts are mainly manufactured from active substances, for example the use of silica-alumina for catalytic cracking reactions. Impregnated catalysts are obtained by impregnating a pre-formed support with the active phase, with the method being commonly used in the preparation of hydrotreatment catalysts. Mixed-agglomerated catalysts can be manufactured by mixing a powdered support with the active substance and combining them by agglomeration, as is quite often performed in the preparation of hydrotreatment catalysts.

Bennett *et al*. [43] studied the effect of catalyst preparation technique upon the product profiles and rates of 2-pentyne hydrogenation. They used a 1wt% Pd/Al_2O_3 catalyst supplied by Johnson Matthey. Catalyst Type A consisted of θ alumina particles that were ground to a powder before impregnation with palladium, whilst catalyst Type B was comprised of the same support, but ground after impregnation. It was found that catalyst Type B led to a much higher rate of reaction owing to a higher metal dispersion of palladium. Chemisorption measurements revealed that Pd on catalyst Type A had an active particle diameter of 8.1 nm and dispersion of 13.8 % whilst on catalyst Type B the active particle diameter was 1.6 nm and metal dispersion was 68.4%. Solvent selection was shown to strongly influence the reaction rate and selectivity in heptane, isopropanol and 50/50 mixtures of these solvents. The reaction in heptane was much faster than in isopropanol, which was through to be due to enhanced substrate solubility. A mixed solvent consisting of 50/50 heptane/isopropanol was found to lead to intermediate rates to those of the pure solvents, but selectivity was superior, with cis/-trans and alkene/alkane selectivities much higher than the pure solvents. The effect was further investigated by carrying out adsorption experiments of the reagents in the different solvents. These indicated that the 50/50 heptane/isopropanol gave a higher degree of adsorption of alkyne on the catalyst than in either of the pure solvents. This can help to explain the high alkene/alkane selectivity, since a high coverage of the surface with alkyne is less likely to lead to re-adsorption of free alkene and further hydrogenation. Also, a strong alkyne adsorption may lead to lower concentration of adsorbed hydrogen on the surface, and may slow the hydrogenation rate whilst improving the selectivity.

The goal of increasing reaction rate, selectivity and catalyst lifetime drives the requirement for further research into new catalytic materials. Almost monodisperse metal nanoparticles of less than 100 nm size have considerable potential as novel and highly active and selective catalysts [45]. Since these particles have a much higher surface-to-volume ratio than their bulk counterparts, they have a larger fraction of catalytically active atoms on their surface. These atoms are not ordered in the same manner as those in the bulk metal and, since the electrons in nanoparticles are confined in small spaces of a few atoms width, they can give rise to quantum size effects. The methods of synthesizing metal nanoparticles also provide greater control over the size and surface composition of the particles than bulk scale catalysts. Zahmakiran and Ozkar [45] noted that there are two general approaches to the preparation of metal nanoparticles, amongst numerous detailed procedures, these being "top-down" and "bottom-up" approaches. Large particles of bulk metal are disintegrated into nanoparticles using thermal, chemical or mechanical methods in the "top-down" approach. The generation of metal atoms from a metal salt or precursor is followed by agglomeration into nanoparticles in the more common and practical "bottom up" approach. A challenging issue in the synthesis of metal nanoparticles is achieving well-defined shape and close control of particle size, since these parameters control the surface structure, electronic and oxidation states of the particle and thus strongly impact upon the catalytic rate and selectivity. Classical methods of preparing supported metal nanoparticles include ion-exchange followed by chemical

reduction or thermal reduction, co-precipitation, deposition-precipitation, impregnation, electrochemical and photochemical methods. Chemical vapor deposition and atomic layer deposition are gas phase techniques used to encapsulate metal NPs within various types of porous materials. Catalytic nanoparticles find applications in aqueous, organic, biphasic and ionic liquid media. The use of palladium nanoparticles in hydrogenation and other organic syntheses has been summarized in a number of review articles [46, 47].

Creamer *et al*. [48] demonstrated the use of bacterial cells as a catalyst support using various bacterial strains, including *Desulfovibrio Desulfuricans*. The ability of some bacteria to reduce metallic ions has been applied to the recovery of previous metals (Pd(II), Pt(IV), Au(III)) from pure solutions and reprocessing wastes. During bioreduction of metal ions from solution, a layer of metallic nanoparticles becomes deposited upon the bacterial cell [49]. For palladium, a high catalytic activity is displayed by biogenic Pd(0) nanoparticles; 'bioPd', as it has become known, is effective in a range of reactions including the hydrogenation of itaconic acid, 2-butyne-1,4-diol, 2-pentyne, dehalogenation of flame retardant materials and Heck coupling reactions [48–53]. The catalyst preparation involves growing the bacterial culture, harvesting by centrifugation and washing the live cells. They are then treated with an acidified solution of sodium tetrachloropalladate (pH 2–3) prepared to the desired Pd loading.

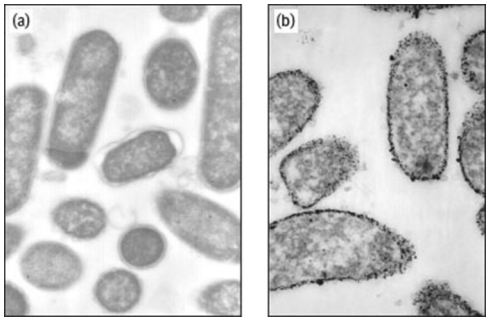

Figure 12: STEM images of D. desulfuricans bacteria (a) before and (b) after impregnation with palladium metal. Reprinted from Bennett *et al*. © [54], with permission from Elsevier.

The cells and solution are stirred under nitrogen followed by hydrogen flows, the latter acting as a reducing environment. The resulting material is recovered washed and dried to produce a powdered catalyst, supported upon dead bacterial biomass. A TEM micrograph showing the bacterial cell with deposits of Pd in the cell membrane is shown in Figure 12. Studies indicated that hydrogenase enzymes near the surface of the bacterial cell are associated with the formation of nanoparticles. They are formed within the peptidoglycan matrix (which contains a sugar-amino acid polymer), located between the two layers of the cell membrane. Particle size may be regulated in the preparation by the ratio of mass of cells to palladium salt. The formed nanoparticles are immobilized and protected from dissolving by becoming entangled within the peptidoglycan matrix. Biomass has a number of attractive features for use as a catalyst support. The precious metals could be obtained from waste sources, including spent car catalytic converters or electronic scrap, since an acidic leachate is required in the preparation process. After the useful lifetime of the catalyst, the metal can be easily recycled by microwaving, sonication or incineration of the biomass. Bennett *et al*. [54] sought to demonstrate the use of bioPd catalyst in a multi-product reaction, the hydrogenation of 2-pentyne, and to study reaction rate and selectivity obtained using this type of catalyst in the stirred tank reactor. The catalyst used was 5 wt % Pd loaded upon *Desulfovibrio Desulfuricans*. The metal particles were found to be evenly dispersed in the cell wall with a fairly even particle size of $\sim$ 1.7 nm. Reaction rates and selectivity were also measured over a conventional Pd/Al_2O_3 catalyst for the purposes of comparison. Figure 13 shows the reactant and product profiles over the 5wt% bioPd catalyst. The 5 wt % bioPd catalyst was found to give a slower initial rate of reaction in isopropanol solvent, with only 30% of the rate observed over a 5wt% Pd/Al_2O_3 catalyst. However, a high selectivity was displayed by the biomass-supported catalyst, with pentene/pentane ratios in the range of 8–14 and cis-trans product ratios in the range of 6–14. Figure 14 shows the pentene/pentane and cis/trans selectivity ratios over 5 wt % bioPd, 1 wt % and 5 wt % Pd/Al_2O_3 in isopropanol solvent. The conventional 5 % Pd/Al_2O_3 catalyst gave very high pentene/pentane and cis/trans ratios at low conversions of 2-pentyne, but these fell sharply as the reaction proceeded and became slightly lower than those observed with the bioPd at alkyne conversions greater than 70 %. At high alkyne conversion of 92 %, the 5 wt % Pd/Al_2O_3 gave a cis/trans ratio of 2.0 and pentene/pentane selectivity of 2.0, whereas the 5 wt % bioPd gave respective selectivity values of 2.5 and 3.3. Although the reaction rate could not match the Pd/Al_2O_3 catalyst, it had been demonstrated that bioPd could be applied with favorable selectivity in a multi-product hydrogenation reaction. It was also demonstrated that the bioPd could be separated from the product mixture and recycled for use in a subsequent hydrogenation, in which it remained active.

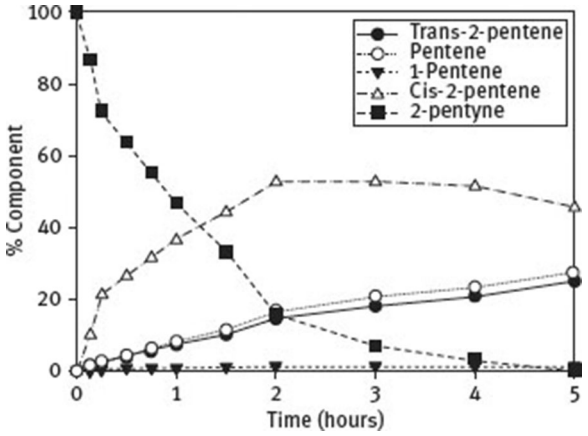

Figure 13: Concentration profle for 2-pentyne hydrogenation in isopropanol using 5 wt % bio-Pd as a catalyst and a stirring speed of 445 rpm. The bacterial strain used in the catalyst preparation was *D. desulfuricans*. Reprinted from Bennett *et al*. © [54], with permission from Elsevier.

The concept of rational design of catalyst surfaces may be extended to cover engineering of active site distribution to try to achieve the desired product selectivity in a particular reaction. Recent work showed that selectivity control can be achieved for heterogeneous catalysts by control of metal particle size and topography. Particular crystal facets upon a metal surface may influence the reaction behavior; for example, in partial hydrogenation of alkynes, it is known that alkyne hydrogenation is favored on terraces, while alkene hydrogenation or isomerization is favored on surface defect sites, such as corners or edges, as illustrated in Figure 15 [55]. Schmidt *et al*. [56] reported differences in the catalytic activity of equally sized nanoparticles of platinum with different shapes, namely cubic, cubooctahedral and octahedral. In the absence of a chiral modifier, each of the three types of NPs gave similar activity and selectivity in the racemic hydrogenation of ethyle pyruvate. However the addition of a chiral modifier such as cinchonidine or quinine were able to give different effects depending upon the NP shape, with the reaction being observed to be faster with increasing ratio of Pt 111]/Pt 100 . The cinchonidine modifier was found to adsorb more strongly to certain types of active site (Pt 100) than other sites (Pt 111 face), leading to hydrogenation and degradation of the modifier. Therefore an ideal catalyst for activated ketone hydrogenation should contain mainly Pt 111 terraces, since this type of crystallographic face gives rise to higher enantioselectivity with higher stability of the modifier. Bennett *et al*. [50] carried out a study of selectivity control of Pt catalysts in 2-butyne-1,4-diol hydrogenation using two routes: (1) In conventional Pt/C catalysts bismuth was used as a site blocking agent, which was able to selectively cover step sites. (2) In bioPt catalysts prepared using *Eschericihia coli*, residual molecular fragments, left over after chemical cleaning and subsequent separation from the bacterial support were used as a site blocker, being found to accumulate preferentially at crystal defect sites. In the second case, the bioPt is prepared by depositing the Pt on the bacterial cell, followed by the usual drying and grinding, then chemical processing, to remove most of the biomass, particularly from terrace crystal sites. Selective poisoning of a catalyst achieved using residual biomass, rather than irorganic counterpart chemical modifiers such as lead or bismuth, could be an advantage because of reduced toxicity. Figure 16 illustrates the butenediol selectivity as a function of alkene conversion for both the Pt/C system with and without Bi poison and the BioPt catalyst before and after chemical cleaning. Bi-poisoned 5 % Pt on graphite gave butenediol selectivity greater than 90 % at low alkyne conversion below 20 %, but only a low rate of reaction (20 % of the alkyne converted after 2 hours). The butenediol selectivity with chemically processed bioPt was of the order of 70 % but with a faster rate (45 % of the alkyne converted after 2 hours). The butene diol selectivity of the Pd/C treated with Bi (~ 90 %) was substantially higher than Pd/C without modifier (~55 %), as was the selectivity over the chemically processed bioPt (~ 70%) compared with the unmodified bioPt (~ 50 %). It was suggested that biogenic catalysts may function similarly to Lindlar catalysts, which are often used in the selective hydrogenation of alkynes, where a poison of the metal sites is used, but the biogenic catalyst avoid the potential risks of using toxic heavy metals such as lead. Related work by Attard *et al*. [52] showed that the use of defect site blocking modifiers such as bismuth or polyvinylpyrrolidone (PVP) could be used to effect large increases in selectivity to the semi-hydrogenation product during the hydrogenation of alkynes. This was again a result of selective site blocking, in particular covering defect sites to leave behind mainly Pt 111 terrace sites. It was found that alkynes strongly associate with defect sites to produce a durable surface complex that allows for over-hydrogenation of the intermediate to produce an alkane. Covering the defect sites using bismuth or PVP was found to eliminate the defect sites associated with over-hydrogenation and thus a substantial increase in selectivity towards the alkene product was observed. The results were corroborated by advanced spectroscopic data obtained using shell-isolated Raman spectroscopy (SHINERS) and electrochemical data obtained by cyclic voltammetry.

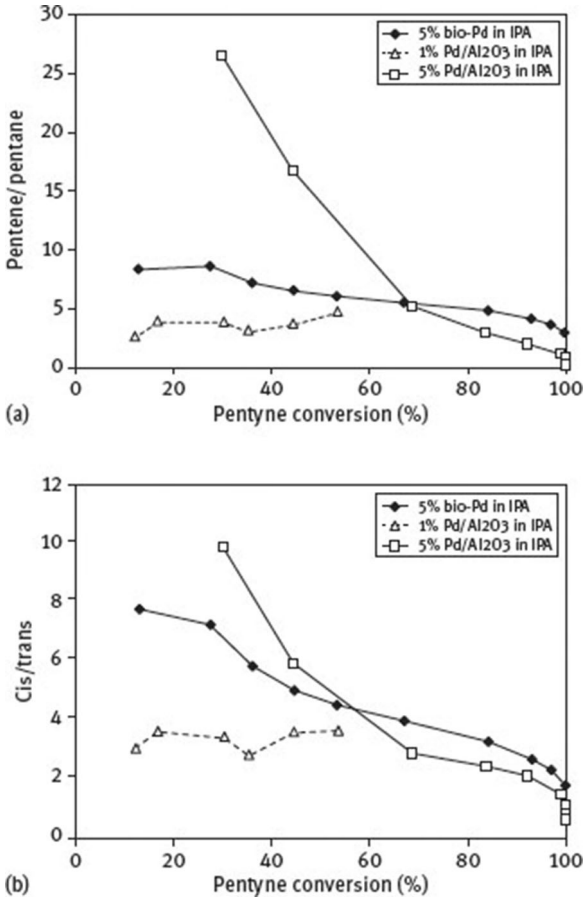

Figure 14: (a) Pentene/pentane versus 2-pentyne conversion for hydrogenations catalyzed by 5 wt % bio-Pd and 1 % and 5 % Pd/Al_2O_3 in isopropanol. (b) Cis/trans-2-pentene ratio versus 2-pentyne conversion for hydrogenations catalysed by 5 wt % bio-Pd and 1 % and 5 % Pd/Al_2O_3 in isopropanol. Reprinted from Bennett *et al*. © [54], with permission from Elsevier.

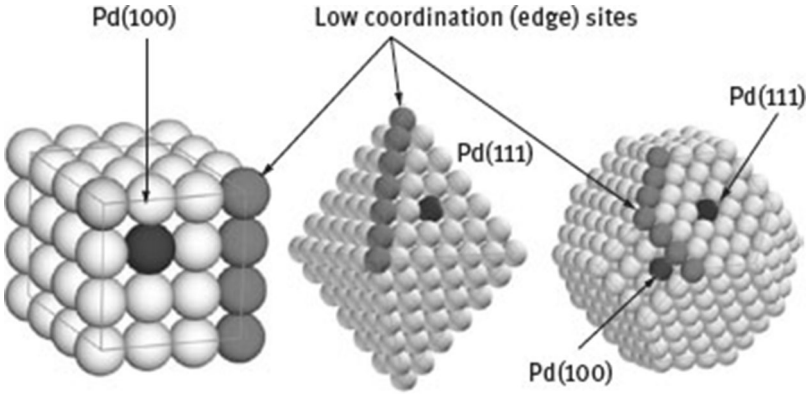

Figure 15: Illustration of the crystallographic facets of palladium, showing edge and terrace sites (Pd(100) and Pd(111)). Adapted from Crespo-Quesada *et al*. © [55], with permission of American Chemical Society.

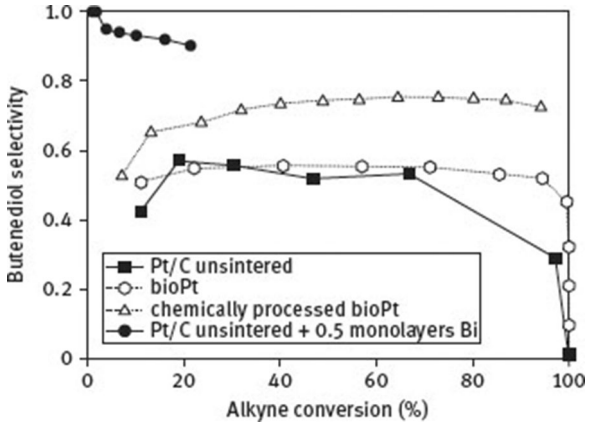

Figure 16: Butenediol selectivity versus alkyne conversion using four different platinum catalysts with increasing occupation/blockage of defect sites. Reprinted from Attard *et al*. © [52], with permission from American Chemical Society.

2.5 Oxidation reactions in the slurry reactor

Over the last twenty years, there has been increasing interest in the development of catalytic oxidation processes for the production of bulk and fine chemicals. Catalytic oxidation covers a vast range of applications, with some of these being reviewed by Mills and Chaudhari [19]. Some examples of liquid phase oxidation in industry include oxidation of *p*-xylene to terephthalic acid, cyclohexane to adipic acid, *n*-butane to acetic acid, epoxidation of propylene to propylene oxide and hydroxylation of phenol to hydroquinone and catechol, as well as a range of catalytic oxidation processes for the treatment of organic and inorganic wastes. The traditional approach in oxidation reactions was to use stoichiometric oxidizing agents such as permanganate, dichromate, manganese dioxide and nitric acid, which are toxic and create large volumes of waste material. Therefore, catalytic oxidation has provided an attractive alternative to these processes, driving the development of new catalysts capable of operating under milder conditions with a minimal amount of undesirable by-products being formed. The multiphase character of working with liquid phase reactants, products and air or oxygen poses similar challenges to the design of hydrogenation reactors, in terms of mixing, mass transfer and kinetic processes. Safety must be paid particular attention due to the constraint in limits of operation with regard to oxygen and organic concentrations employed. Oxidation processes are distinguished by a number of features, which include the use of critical oxygen concentration, below the flammability limit of the oxygen-organic mixture; this may be a limiting factor in terms of the reaction rate achieved. However, the use of molecular oxygen via air or enriched air is relatively cheap and much less toxic than strong stoichiometric oxidizing agents. Heterogeneous catalysts can efficiently use molecular oxygen to produce only water as a side-product. This proves to be cost efficient because supported catalysts can be recovered and recycled, or can be used in continuous flow reactors [57]. Control of reaction temperature is another significant consideration, since many oxidation reactions are strongly exothermic.

Since the mid-1990s, much attention has been focused on the use of supported gold catalysts for oxidation reactions [58]. The breakthrough work of Haruta *et al*. [59] showed that nanocrystals of Au supported on oxides with a very effective catalyst for CO oxidation at low temperature, whilst Hutchings and Grady [60] predicted – and later the group of Hutchings verified [61] – that cationic gold would be an effective catalyst for the hydrochlorination of acetylene. Since then, research on gold catalysis has been greatly increased, and gold catalysts developed encompass reactions such as the oxidation of glycerol, cyclohexane and alcohols [58].

Heterogeneous catalysts for oxidation reactions are attracting the interest of industry and academics; one particular class of such reactions being the oxidation of alcohols to carbonyl compounds [62–64]. The acknowledged reaction mechanism for platinum group metals is the loss of two hydrogen atoms from alcohol, forming the carbonyl compound via a dehydrogenation pathway before the adsorbed hydrogen reacts with molecular oxygen to form water [62, 65]. A crucial issue concerns the best catalyst selection and design, and how to ensure the catalyst has a long lifetime without significant deactivation problems. PtBi/Carbon is also a promising catalyst for alcohol oxidations, since bismuth acts as a promoter of selectivity for the alcohol oxidation [66, 67]. However, the catalyst can be deactivated through various processes such as over-oxidation, leaching or agglomeration of metal and by-product poisoning [63, 65]. The strong adsorption of an excess of oxygen upon the metal surface occurs in over-oxidation, preventing the alcohol from adsorbing on the active sites. Leaching of the active metal into solution may occur, depending on the substrate used, whilst sintering leads to the migration of small particles to form large agglomerates with decreased surface area and activity [66, 68]. Com-

ponent inhibition may occur when the reactant, product or by-products adsorb on the metal surface leading to blockage of the active sites [69, 70]. This can occur is the carbonyl product strongly adsorbs on the metal.

The oxidation of alcohols is an important class of oxidation reactions, although different alcohols such as vinyl, allylic, aromatic and aliphatic display differing levels of reactivity over noble metal catalysts [64]. Aliphatic alcohols are known to be particularly resistant to oxidation [71, 72]. Mounzer *et al*. [73] investigated the heterogeneous oxidation of 2-octanol on 5 wt% Pt-1 wt % Bi/Carbon catalyst as a case study. Reactions were carried out in a baffled stirred autoclave of 500 ml volume, whilst studies of ketone adsorption upon the catalyst were carried out in a laboratory scale glass flask fitted with a condenser. Oxidation of 2-octanol was carried out at atmospheric pressure with air as an oxidant, temperature at 343 K and using solvents heptane, *p*-xylene and dioxane and mixtures of heptane-dioxane. Using pure solvents such as heptane and *p*-xylene, the reaction rates were shown to start quite fast initially, but rapidly decrease shortly after the start of the reaction due to poisoning by product adsorption. It was shown that pre-treatment of the catalyst surface with ketone also led to a deactivation of the catalyst, demonstrating that this effect could also occur during the reaction due to product formation. To decrease the amount of ketone adsorption, a solvent was sought with greater solubility of 2-octanone to enhance ketone desorption and leave more active sites available for reaction. Various solvents including DMSO, *p*-xylene, dioxane and dioxane/heptane mixtures were investigated for this purpose and adsorption studies carried out to determine the equilibrium uptake of 2-octanone in each solvent or mixture. Figure 17 displays the effects of heptane-dioxane solvent mixture composition on the reaction rate and ketone adsorption coefficient. The lowest amount of ketone adsorption occurred at a 16–18 % v/v mixture of dioxane in heptane, and corresponded to the maximum observed rate of oxidation. The effect of using mixed solvents could influence oxygen solubility in the liquid phase, although the effect of pressure in the range 1–4 bar upon the reaction showed a weak effect of oxygen solubility upon the reaction rate. Therefore, it was concluded that the maximum reaction rate occurred because the ketone was removed from the catalyst surface by the corresponding particular solvent composition. The use of mixed solvents may be used to tune the product adsorption properties, with 2-octanone having a long carbon chain resulting in a lipophilic character but also the carbonyl bond exhibiting polarity that is responsible for bonding with the metal. The experimental rates were fitted by a Langmuir-Hinshelwood expression, which include a ketone adsorption term in the denominator:

$$R = \frac{k_3 K_1 [A] (K_2 [\mathrm{O}_2])^{0.5}}{\left(1 + K_1 [A] + (K_2 [\mathrm{O}_2])^{0.5} + \frac{[P]}{K_4}\right)^2}, \tag{24}$$

where k_3, K_1, K_2, and K_4 are the reaction rate, alcohol adsorption, oxygen adsorption and product adsorption coefficients respectively. $[A]$ is the alcohol concentration and $[P]$ is the product concentration. Although particular to a case study of 2-octanol oxidation, the results illustrate the complex interplay between kinetics, product adsorption and catalyst deactivation that may occur in selective oxidations.

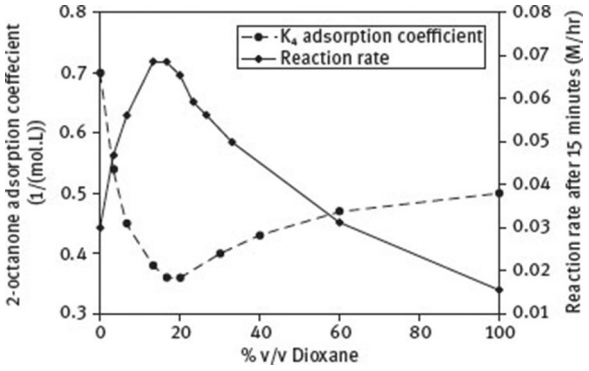

Figure 17: Effects of heptane–dioxane solvent composition upon reaction rate and ketone adsorption coefficient. Reaction conditions: T = 343.15 K; P_{Air} = 1 bar; C_i = 0.248 M; stirring speed = 22.5 s^{-1}. Reprinted from Mounzer *et al*. © [73], with permission from Elsevier.

2.6 Bubble column reactors

Bubble column reactors are a class of slurry reactor in which a gas is bubbled through a column of liquid where it reacts via a chemical or biochemical reaction, typically in the presence of a suspended catalyst. Normally no agitator is used, which offers the advantage of no moving parts, together with good heat and mass transfer, ease

of operation and low operating and maintenance costs. However, backmixing can occur, with the expense of a reduction in product conversion. A high superficial gas velocity (up to 50 cm/s) is used to impart momentum transfer to the slower moving liquid (up to 2 cm/s) to promote mixing and circulation patterns [74]. Bubble columns find application in a range of processes for hydrogenation and oxidation, and are also used for hydroformylation, chlorination, cell growth and bioremediation. Industrial applications include partial oxidation of ethylene to acetaldehyde, liquid phase methanol synthesis, wet air oxidation, Fischer-Tropsch synthesis, maleic acid hydrogenation and a range of biochemical processes including cultivation of bacteria and various cell cultures, also the treatment of sewage. However, bubble columns can be difficult to scale up, since the extrapolation of laboratory scale data to pilot and industrial scales requires similarity criteria that would achieve similar mixing, hydrodynamic performance and thus match conversion and selectivity. Shaik and Al-Dahhan [74] have provided a recent detailed review of the state-of-the-art in scale up methods for bubble column reactors, based on extensive experimental and computation studies. Advances in the understanding of fluid dynamics in the bubble column have resulted from novel measurements and computation modeling efforts.

A number of techniques including hot-wire anemometry, PIV and LDA have been applied to the measurement of velocity and turbulent stresses in the bubble column [75]. However, optical techniques can only be used for low solids loading and gas fraction; therefore, non-invasive imaging techniques for opaque vessels are required. Devanathan *et al*. [15] and Dudukovic *et al*. [75] introduced radioactive particle tracking studies to investigate liquid motion in bubble columns. The technique produces Lagrangian data for the whole column, similar to the PEPT technique reviewed in Section 2.2. The instantaneous velocities, time averaged flow patterns, turbulent stresses and turbulent kinetic energy can be derived from the tracer particle trajectories. CARPT is used to measure the position of a single radioactive particle using a series of scintillation detectors. In order to measure the motion of catalyst particles in slurries or fluidized beds, a tracer particle of equal density to the particles in the system is used, or if measuring the fluid velocity, a neutrally buoyant particle is used. The system is able to measure motion up to frequencies of 20-30 Hz. Computer tomography (CT) was also used to obtain time averages gas holdup profiles in the column cross sections over a range of elevations. The combination of CARPT-CT provided the time averaged flow field and gas holdup distribution in bubble columns. Using the technique, the radial gas holdup profile was observed to be almost flat, with slightly more gas near the center at low gas superficial velocities, whilst the gas holdup profile became almost parabolic in churn turbulent flow. Velocity maps recorded at U_g = 2.4 cm/s, in a 14 cm diameter column [76] showed a single-cell flow circulation pattern, as had also been earlier observed by Devanathan *et al*. [15]. The flow pattern was observed to be quite symmetric about the column axis. Visual observation of the flow in the column indicated that gas bubbles tend to form "swarms" that follow a spiraling motion, rocking from one side of the wall to the other and becoming gradually more evenly distributed at higher levels in the column.

Computational fluid dynamics (CFD) has also been used for the modeling of bubble columns. A review of modeling of bubble column reactors is provided by Jakobsen *et al*. [77]. Two approaches are commonly used: the Euler-Euler formulation and the Lagrange-Euler approach. The Eulerian description of the fluid flow is based on the concept of pseudo-continuum and thus defines a point volume fraction for each of the phases that is representative of the probability of that phase to be present at that particular point in multiple realizations of flow. Each of the phases shares the same pressure field. The force interactions between the phases are allowed by using various effective "volumetric" force functions including drag force, lift and added mass force [78]. Such a model was formulated and solved by Gupta and Roy [78] and validated using data from radioactive particle tracking. Very good agreement was observed for velocity profiles at a high superficial gas velocity of 2.38 mm/s with the selection of suitable drag (Schiller Nauman) and turbulence (RNG k-ε) model. The Lagrange-Euler method involves the solution of the Navier-Stokes equation for the continuous phase and solution for the motion of each of the bubbles by the application of Newton's second law, with the various forces upon the bubble being calculated using the local velocity patterns of the continuous phase. The density and viscosity of the continuous phase are often modified to allow for the low volume fraction of the dispersed phase (bubbles). The two approaches have various advantages and disadvantages, for example the Lagrange-Euler model requires some additional tuning parameters, such as effective diffusivity for the dispersed phase and effective viscosity for the continuous phase [79]. A remaining challenge in the modeling of bubble column reactors concerns the treatment of bubble coalescence and breakage processes, although population balance modeling is starting to be used to represent these phenomena [77].

Many industrial bubble column reactors work in upflow mode, with gas and sometimes liquid (cocurrent operation) being introduced via a sparger at the base of the reactor. In countercurrent operation, the liquid would be introduced at the top of the reactor and flow towards the bottom. The Cocurrent Downflow Contactor Reactor (CDCR) is an exception to the aforementioned operation, in which both the gas and liquid stream are introduced concurrently via an orifice and entry zone at the top of a fully flooded column. The device was developed at the University of Birmingham by Boyes *et al*. [80]. The CDCR was found to give high gas-liquid mass transfer coefficients (k_{la}) via high interfacial area (1000–1500 m^2/m^3) and gas hold up (0.5–0.6), thus making it

suitable for application in catalytic hydrogenation reactions, where is it possible to overcome the hydrogenation mass transfer resistance and make the most effective use of the catalyst [81]. In the upper section of the column, a gas-liquid dispersion is formed by a high velocity liquid jet inlet stream, which prevents a gas pocket from forming. The dispersion is comprised of almost uniformly sized bubbles depending on the liquid and gas used (e.g. H_2/H_2O 3–4 mm). Further advantages of the CDCR include: low power consumption, small containment volume, easy scale up, 100 % gas utilization with operation close to equilibrium, inherent reliability due to no moving parts and tolerance to particles, therefore suitable for use as a slurry reactor [80]. Increasingly stringent regulations regarding wastewater treatment led to the need to develop innovative and more efficient wastewater treatment technologies, required to decompose toxic industrial effluents and to improve discharge water quality. The CDCR has been demonstrated to be an effective technology for wastewater degradation. The use of Advanced Oxidation Processes (AOPs) includes photocatalysis and oxidation to treat organic pollutants. Key to the effectiveness of AOPs is the formation of hydroxyl radicals (HO), which are a powerful oxidizing species for organic compounds in the aqueous phase, with stronger oxidising power than that achievable using single oxidizing chemicals such as chlorine, hydrogen peroxide and ozone [82]. A number of different techniques can be used to generate hydroxyl radicals, with each method involving the use of an oxidant (H_2O_2,O_3,O_2), together with an activating system such as a catalyst, UV light, alkali or another oxidizing species. In photocatalysis, a photocatalytic semiconductor, such as TiO_2, is activated by radiation of suitable energy (*hv*) and wavelength to promote the excitation of electrons, which upon acceptance by oxygen on the semiconductor surface yield unstable superoxide radical ions (O_2^-) and further yielding hydroxyl radicals HO′. Winterbottom *et al*. [82] gave further details of the photocatalytic mechanism. Photocatalysis was investigated for the destruction of phenol using the CDCR by Winterbottom *et al*. [82]. Allowing for all the possible reactions, the general reaction schemes for phenol destruction by photocatalysis could be represented as:

$$C_6H_5OH + {}^{\cdot}OH \rightarrow \text{intermediates} \rightarrow CO_2 + H_2O;$$

and

$$C_6H_5OH + HO_2^{\cdot} \rightarrow \text{intermediates} \rightarrow CO_2 + H_2O.$$

In order to use the CDCR as a photocatalytic reactor, UV lamps were fitted into the base section, with powers of either 30 W or 1.0 kW. The reaction of phenol was carried out at temperatures of 40–50 °C and 202.6 kPa, with operation of the reactor under a closed loop recycle mode with recirculation of the suspended TiO_2 catalyst. Complete degradation of phenol was achieved in as little as 30 minutes reaction time using $O_2/UV/TiO_2$ with a pH of 7.0 or below using the higher powered lamp from solutions containing 100 mg/dm^3 phenol.

An important class of chemicals of environmental concern include nitrogen-containing compounds which are resistant to biological treatment and thus persist after passing through conventional sewage treatment works. These compounds are often encountered in pharmaceutical effluents, generally at microconcentrations. European Community regulations have stipulated discharge limits for a number of such pollutants [83]. 1,8-diazabicyclo[5.4.0]undec-7-ene (DBU) is a recalcitrant compound present in waste water produced from pharmaceutical processes, consisting of a nitrogen-containing tertiary amine that was tested for degradation in a CDCR operating as photocatalytic reactor. The effects of photocatalyst loading, initial reactant concentration, temperature, pH and various combinations of AOPs including UV, O_2, H_2O_2, and TiO_2 upon photocatalytic degradation of DBU were investigated. A slurried granular catalyst (Degussa VP Aeroperl P25/20) was selected for ease of filtration from the treated water. The reactions were carried out at 40–60 °C and 1 barg using a 1.0 kW UV lamp mounted in the base of the reactor, and operation of the reactor in closed loop recirculation mode. It was found that a combination of TiO_2, UV radiation, and O_2 gave the most rapid degradation and mineralization of DBU in comparison with other combinations of AOPs. Optimization of the reaction conditions led to 100 % degradation of DBU in 45min, using a 1kW lamp, 0.5 g/dm^3 TiO_2, 100mg/dm^3 DBU, 1 barg, 50 °C, and pH of 3.17. Figure 18 (a) displays the reactor set up, in which a slurry catalyst may be optionally used in place of the reticulated foam monolith, and Figure 18 (b) shows the degradation profiles of DBU with the slurry catalyst. The formation of intermediates in the degradation process was considered, with use of GC-MS to detect the various compounds occurring during oxidation. It should be noted that some of the intermediates formed during photocatalytic degradation of wastes could be more hazardous than the starting material, so it is important to measure the destruction of total organic carbon (TOC), rather than just the starting compound. A first order reaction model was able to describe the degradation process. Ochuma *et al*. [84] also carried out a similar optimization study for the destruction of 2,4,6-trichlorophenol as an alternative model pollutant in industrial wastewater. A potential drawback of using slurry catalysts is the necessity for installation of a filtration system to separate the catalyst from treated wastewater. Ochuma *et al*. [85] demonstrated the application

of a reticulated foam monolith catalyst, comprised of TiO_2-coated alumina, installed in the annular space between the centrally installed UV lamp and internal wall of the reactor (Figure 18 (a)). The oxidation of the model pharmaceutical waste DBU was again tested for evaluation of the reactor performance. The results indicated that a 12 wt % TiO_2 coated reticulated foam catalytic reactor could achieve a TOC conversion of approximately 23 % within 60 minutes reaction time. Depending on the basis for comparison, as to whether equivalent mass concentration in slurry form as the monolith TiO_2 loading or optimal slurry concentration for the quickest degradation is used, the former comparison indicates that the reticulated foam is more effective than the slurry reactor, whilst the latter indicates that the slurry reactor is preferable. The use of a reticulated foam monolith has the advantage of avoiding catalyst filtration and separation problems from the treated water.

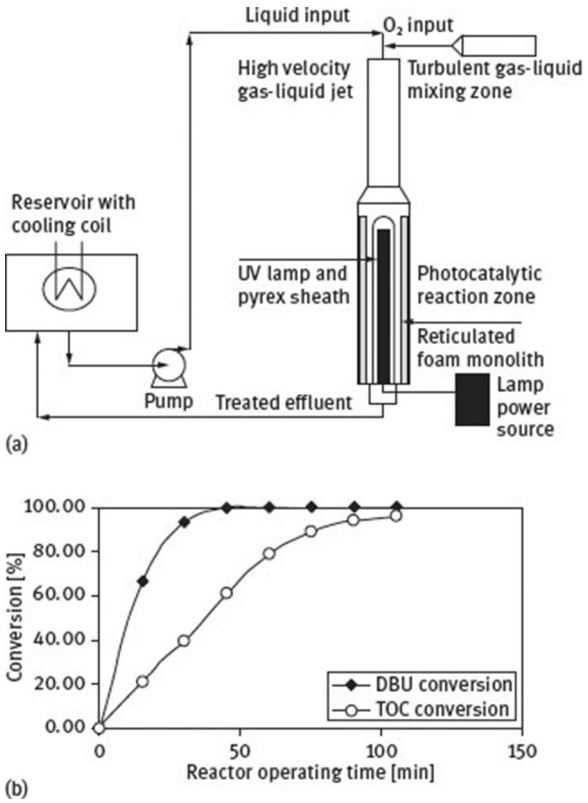

Figure 18: (a) Experimental set-up of the photocatalytic CDCR showing optional reticulated foam monolith installed around the UV lamp. (b) Degradation profile of DBU in the photocatalytic slurry bubble column reactor (pH = 3.17, T = 50 °C, flow rate = 0.1 dm^3/min, catalyst loading = 0.5 g/dm^3). Reprinted from Ochuma *et al*. © [83, 85], with permission from Elsevier.

3 Trickle bed reactors

Trickle bed reactors are packed bed catalytic reactors operating in concurrent down-flow, which have attracted a large amount of industrial interest owing to their importance in the chemical, petroleum and petrochemical industries. As such, trickle bed reactors have been the subject of many reviews [79, 86]. Trickle beds are typically used in the hydrotreatment of fuels, including hydrodesulphurization, hydrodemetallation, hydrodenitrification [87], a range of selective hydrogenation of substrates including as selected examples; C_4 olefins [88], maleic anhydride [89], α-methyl styrene [90] and biological processes such as wet air oxidation of waste water and model pollutant effluents [91].

3.1 Theory and flow regimes

Trickle bed reactors may be operated under a range of flow regimes that may be summarized as:

– Spray flow: where liquid exists as droplets and gas flows continuously;

– Trickle flow: liquid rivulets and films flow over catalyst particles with gas as continuous phase;

– Pulse flow: consisting of intermittent flows of gas and liquid rich zones through the reactor;

– Bubble flow: where the liquid flow is continuous with dispersed bubbles.

A detailed review of liquid distribution and flow texture in the trickle bed has been provided by Maiti *et al*. [92]. Figure 19 shows a cut-away diagram of the trickle bed reactor. The flow regime in the trickle bed reactor is typically determined using a flow map, as shown in Figure 20 (adapted from Baker [93]), where the axes are presented in terms of the liquid and gas mass velocities. Laboratory scale reactors typically operate within the lower range of the trickle flow, whilst many industrial processes such as hydrotreatment operate in pulsed flow due to the higher energetic interaction between the phases [94]. The pulsed regime is attractive for industrial operation due to the intensified processes for heat and mass transfer, where the periodic passage of liquid and gas waves promotes uniform liquid distribution through the packing [95]. This is important to achieve a high wetting of the exterior surface of the catalyst particle, since incomplete wetting effects can lead to a lower reaction rate than expected [86]. Due to the complex flow regimes that may occur, the design of trickle bed reactors is complex, but the key parameters that need to be considered for design include pressure drop, liquid holdup and wetting efficiency. A detailed review of trickle bed hydrodynamics is beyond the scope of this chapter, and therefore this review considers some of the important factors that may need to be considered in the scale up and design of trickle bed reactors from lab to pilot and industrial scale.

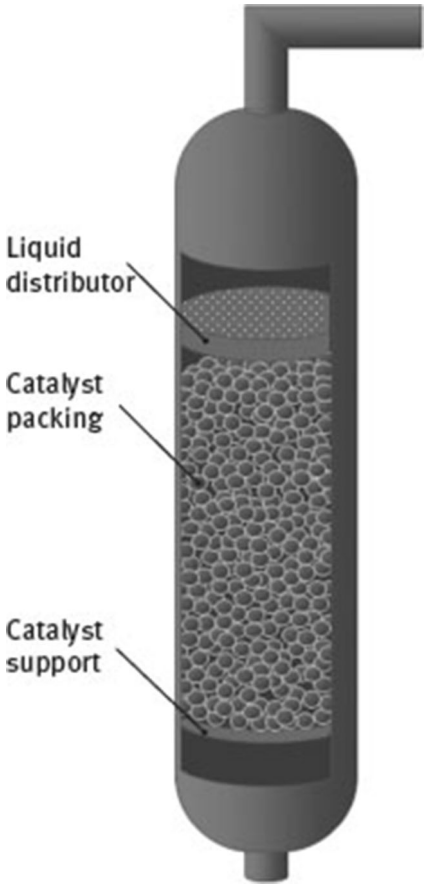

Figure 19: Schematic diagram of a trickle bed reactor.

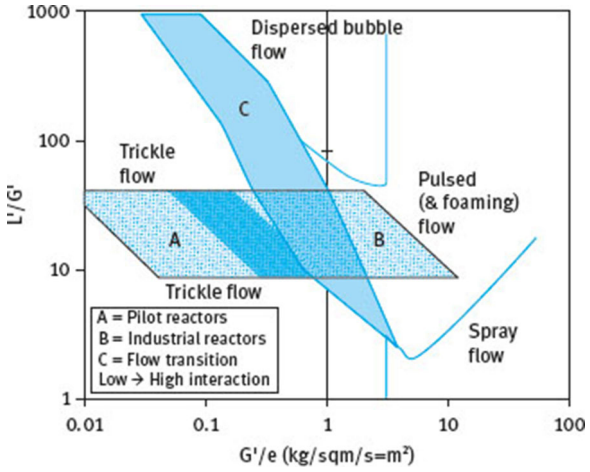

Figure 20: Flow map for a trickle bed reactor, after Baker [93]. Notation: L', liquid mass velocity; G', gas mass velocity; e, voidage.

3.2 Overall rate model

The basic transport and reaction steps for trickle bed reactors are identical to those already presented for slurry reactors, although the hydrodynamics of contacting the various reacting phases is different. The main differences in the overall design equations result from: (i) the different correlations required to calculate the mass transfer coefficients; (ii) the greater likelihood that gas absorption resistance is significant, since dilute gases are sometimes used to prevent runaway of exothermic reactions; and (iii) the need to consider effects of diffusion resistance of the liquid component B as well as the dissolved gas phase component A (Winterbottom and King [2]). The derivation steps of an overall reaction rate model for the trickle bed have been presented by Winterbottom and King [2] and Fogler [5]. It should be noted that the reaction rates for the trickle bed are often presented per unit mass of catalyst, whilst for the slurry reactor the rates are per unit volume of slurry. This results in the introduction of the term $1/((1-\varepsilon_b)\rho_P)$ in the below equations, where ε_b is the bed voidage and ρ_p is the density of the catalyst pellets. The additional step that must be considered for the trickle bed compared to the slurry reactor is the transport from the bulk gas phase to the gas-liquid interface. The rate of transport per unit mass of catalyst is:

$$R'_A = k_g a_i \frac{1}{(1-\varepsilon_b)\rho_p}\left[C_{Ag} - C_{Ai}\right], \tag{25}$$

where k_g is the gas phase mass transfer coefficient, C_{Ag} is the bulk gas phase concentration of A and C_{Ai} is the concentration of A at the interface. Similar equations may be written for the other mass transport and reaction steps, as for the slurry reactor. Reaction is assumed to be first-order in dissolved gas A and in liquid phase reactant B. Combining the various mass transfer and reaction equations leads to the overall rate equation for gaseous reactant:

$$R'_A = \frac{1/H}{\frac{(1-\varepsilon_b)\rho_c}{Hk_{gA}a_b} + \frac{(1-\varepsilon_b)\rho_c}{k_l A a_b} + \frac{1}{k_{cA}ac} + \frac{1}{\eta k C_{BS}}} C_{Ag} = k'_{gA} C_{Ag}, \tag{26}$$

the symbols are as defined for the slurry reactor in Section 2.1, with k being a second order rate constant and CB_s the concentration of liquid phase reactant at the exterior surface of the catalyst particle. k'_{gA} is an overall transfer coefficient for the gas A into the pellet. In terms of design, the catalyst weight must be calculated for a particular flowrate and conversion. Considering the trickle bed as a heterogeneous plug flow reactor, the differential material balance then gives, for the change dF_A in the molar flow rate of A on passing through the catalyst mass dW:

$$\frac{-dF_A}{dW} = R'_A = k'_{gA} C_{Ag}. \tag{27}$$

In the case of reactant A being mass transfer limiting the catalyst mass may be found by integration of the above equation to give:

$$W = \frac{-v_g}{k'_{gA}} ln \left[\frac{1}{1 - X_A}\right], \tag{28}$$

where v_g is the volumetric flow of the gas stream, and X_A is the conversion of reactant A. A similar analysis for the rate of diffusion and reaction of B inside the catalyst pellet leads to the expression:

$$R'_B = \frac{1}{\frac{1}{k_{cB}a_c} + \frac{1}{\eta k C_{AS}}} C_{Bb} = k'_{lB} C_{Bb}, \tag{29}$$

where k_{cB} is the external mass transfer coefficient from the liquid to solid for reactant B, and C_{Bb} is the bulk concentration of reactant B in the liquid phase. k'_{lB} is the overall transfer coefficient of reactant B. A differential balance for B leads to:

$$\frac{-dF_B}{dW} = R'_B = k'_{lB} C_{Bb}. \tag{30}$$

In case of B becoming mass transfer limiting, the catalyst mass required may be calculated by integration of the above equation to give:

$$W = \frac{-v_l}{k'_{lB}} \ln \left[\frac{1}{1 - X_B}\right], \tag{31}$$

where v_l is the liquid volumetric flowrate, and X_B is the conversion of liquid phase reactant B. Summaries of some of the many correlations for the mass transfer coefficients for trickle beds have been presented by Winterbottom and King [2] and Fogler [5]. The above equations are shown here to demonstrate that the conversion in the trickle bed reactor is a complex interplay between various mass transfer steps and kinetics. Gas-liquid, liquid-solid or internal diffusion in the catalyst pellets may influence the reaction rate, in addition to the intrinsic reaction kinetics, and therefore scale up of the reactor requires a detailed understanding of the particular regime of operation.

3.3 Imaging of gas-liquid flows

As outlined in Section 3.1, understanding the flow regime of operation and transition between trickle and pulsing flow is an important consideration for the operation of industrial reactors, which benefit from enhanced heat and mass transfer effects of operation in a high interaction regime, such as pulsed flow. The Gladden group has developed Magnetic Resonance Imaging (MRI) methods to probe hydrodynamic features of trickle bed reactors such as the onset of pulsing and changing liquid holdup during periodic operation, and mapping of chemical conversion in gas-liquid-solid reactors. To study the onset of pulsing in the trickle bed, rapid 3D MRI was applied to investigate the spatial distribution of liquid in the bed as a function of time, which is able to clearly determine the regions of the bed that are in trickle flow, with constant gas-liquid distribution, and the regions that have moved into unstable flow, with changing gas-liquid distribution characteristic of pulsing [96]. The work has been reviewed by Gladden *et al.*, including details of the development of the MRI techniques used [97, 98]. The implemented trickle bed had a column diameter of 45 mm and catalyst support pellets of 1–3 mm dimension. The formation and development of these pulses with increasing liquid velocity was detected by MRI. The technique was also able to detect fluctuations in the liquid films flowing over the catalyst pellets, which may lead to the formation of local scale pulsing in the reactor. The basis of the technique briefly involved acquiring successive 3D images of the bed, showing the liquid distribution at that instant. A series of 3D images of a 60 mm^3 bed volume with resolution 3.75 mm (x) × 3.75 mm (y) × 1.87 mm (z) were acquired at a rate of 3.6 frames per second, with six series of eight consecutive images being acquired for each flowrate investigated. The standard deviation of the signal intensity associated with each voxel of the image through the series of acquired images was calculated in order to quantify the stability of the liquid distribution in the bed, thus building up a 3D map of standard deviation values. The trickle flow regime is represented by a standard deviation value of ~ 0, whilst unsteady gas-liquid distribution associated with the onset of pulsing is represented by a standard deviation of ≥ 1. A typical standard deviation map is shown in Figure 21, from which the spatial extent of local pulsing regions can be identified as the bed moves from the trickle to pulsing regime. The number of voxels associated with unsteady state liquid content was found to increase with increasing liquid velocity.

Film instabilities in localized areas of the bed were found to propagate with increasing liquid velocities, such that local regions of instability merged together at the transition from a trickle to pulse flow regime. Related studies considered how the MRI results relate to pressure drop and conductance measurements of the onset of pulsing that would be performed for larger, pilot and industrial scale reactor beds [99]. It was found that the pressure drop and conductance measurements only respond after the bed has moved into the fully pulsing region, whereas the MRI technique is able to detect the onset of pulsing. Similar techniques were also applied to the study of periodic operation of the trickle bed reactor. Since reactions in the trickle bed may be controlled by mass transfer processes outlined in Section 3.2, the operation in the periodic model offers the possibility of enhancing the reaction performance by switching on and off the gas or liquid flow, so as to periodically reduce the mass transfer resistances. MRI imaging of the bed was used to calculate the drainage profiles of the bed as a function of time, together with drainage profiles of local channels within the bed. The overall bed showed a gradual and smooth drainage profile after the liquid flow was turned off; however, while some local liquid-catalyst drainage patterns followed the overall pattern for the bed, other voids in the bed showed marked variation from the overall drainage profile, illustrating that local heterogeneities of behavior can occur.

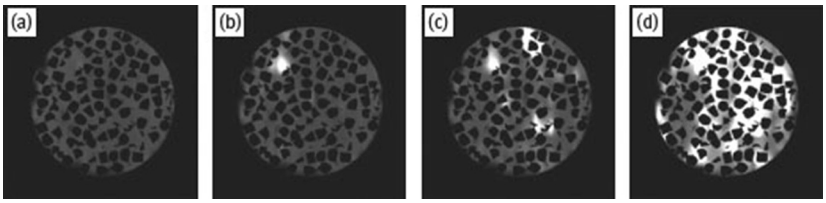

Figure 21: Identification of the location and size of local pulses within the trickle bed determined by MRI. A high spatial resolution image (in-plane spatial resolution 175 μm × 175 μm; slice thickness 1 mm) was overlayed with a standard deviation map calculated from images acquired at a spatial resolution of in-plane spatial resolution 1.4 mm × 2.8 mm and slice thickness 2 mm. The standard deviation maps were linearly interpolated to the same in-plane spatial resolution as that of the high-resolution data. Images are shown for a constant gas velocity of 112 mm s^{-1}, and the data were recorded as a function of decreasing liquid velocity. The liquid velocities are (a) 2.8, (b) 3.7, (c) 6.1, and (d) 7.6mm s^{-1}. Reprinted from Gladden *et al*. © [98], with permission from American Chemical Society.

The development of magnetic resonance was also applied to chemical mapping of conversion and selectivity within the trickle bed reactor [100], which offered the potential to understand spatial variations in activity and selectivity within the bed for the first time. Such heterogeneities could result from spatial variations in hydrodynamics and mass transfer, as mentioned above. Rather than observing the ^{1}H nucleus, ^{13}C observation was used due to easier spectral assignment, with less overlapping of the peaks compared with ^{1}H. ^{13}C Distortion Enhancement Polarization Transfer (DEPT) MRI was thus applied to the study of 1-octene isomerization and hydrogenation in the trickle bed reactor over a 1 wt % Pd/Al_2O_3 catalyst. This particular reaction was chosen for study since it occurs rapidly under conditions of low temperature, so that a substantial amount of isomerization and hydrogenation occurred during a single pass over ~ 3 cm bed length during the experiment. Upon the liquid reaching the catalyst bed, the spectra displayed olefinic and aliphatic peaks, which were quantified to determine the components present within the corresponding region of the bed. The profiles of 1-octene, *n*-octane, 2-octene and 3,4-octene as a function of position in the trickle bed were calculated, illustrating the conversion levels at different penetration distances into the catalyst bed. Such non-invasive measurements are likely to be highly useful in verifying models of the trickle bed reactor.

3.4 Scale up and modeling

The issue of scale up is important for the successful design of commercial reactors based on laboratory data, whilst 'scale down' refers to testing of a new catalyst or feedstock in a laboratory reactor for potential use in an existing industrial scale reactor. It is desirable to match the space velocities of large and small reactors in order to relate the reactant conversion in laboratory scale reactors to those occurring in industrial reactors [101]. Dilution of the catalyst bed with fines is a widely used method to try to achieve this aim, whereby voids between the catalyst pellets in the laboratory scale reactor are filled with small, inert, nonporous particles of approximately $\frac{1}{10}$ the catalyst pellet diameter. Kulkarni *et al*. [101] carried out a study of residence time distribution in trickle beds with porous and non-porous pellets, with and without fines dilution. The dispersion coefficient in the bed was found to decrease by up to 50 % for the bed with fines, compared with an undiluted bed. This suggests that the flow tends closer towards plug flow upon dilution of the catalyst bed with fines, compared with the undiluted bed. The RTD for porous particles showed a longer tail than for non-porous particles because of the holdup of liquid in the catalyst pores.

Iliuta *et al*. [102] developed an axial dispersion-exchange model (ADEM) allowing for transient diffusion within the pores of catalysts. In the trickle bed reactor, films of liquids may be flowing over the outside surfaces of catalyst pellets, whilst liquid bridges may also become trapped in confined voids where particles come into contact with each other. Iliuta *et al*. [102] denoted these regions of liquid as respectively dynamic and static zones. Mass transfer was assumed to occur from the dynamic liquid to static liquid and in turn to liquid inside the catalyst pores. Kulkarni *et al*. [101] found that the model could represent a good fit of RTD data in beds of porous particles diluted with fines. Iliuta *et al*. [103] subsequently formulated a 1D two-fluid hydrodynamic model to approximate two-phase flow in the trickle bed, allowing for the effects of partially wetted catalyst.

Significant complications in design of trickle bed reactors can occur due to a change in phase of the reactants and/or products. A design of the catalytic reactor based on the assumption of liquid phase wetting of the catalyst particles may lead to erroneous results if some of the reacting components are volatile and prone to evaporation [104]. In the event of an exothermic reaction, evaporation of the reactants may occur, leaving previously wetted catalyst particles with dry zones and depletion of the liquid phase reactant. On the other hand, when operating with vapors at high pressure within the confines of a porous catalyst, capillary condensation may lead to the formation of liquid pockets below the normal dew point of the bulk vapor. A review of this phenomenon and its effect upon catalyst particles has been provided by Ostrovskii and Wood [105]. Wood and co-workers utilized pore network modeling in combination with the Kelvin equation to predict the distribution of catalyst pores filled with liquid by capillary condensation in vapor phase reactors [106, 107]. They solved diffusion-reaction network equations and determined – using percolation theory – the fraction of pores accessible to the vapor phase within the catalyst pellet. Assuming that the condensed liquid blocked regions of the catalyst where vapor phase reactions would otherwise occur, a reduction in the catalyst effectiveness factor was observed at low values of the Thiele modulus. A model proposed by Khadilkar *et al*. [104] allowed for wet and dry zones of the catalyst surface together with phase changes occurring due to evaporation and condensation effects, such as may be encountered in the hydrogenation of cyclohexane. The model incorporated pellet and reactor scale submodels. Flow, reaction and transport phenomena were accounted for using multicomponent diffusion theory based on the Stefan-Maxwell formulations. It was shown that multiple steady states may occur, depending on the operating conditions and history of the reactor operation, which were confirmed by comparison with experimental data. For example, at low hydrogen to cyclohexene feed ratios, a lower conversion and reaction rate occurred (Figure 22), showing that the catalyst remains in an internally fully wetted conditions throughout the reactor. Low rates are observed for the mostly fully wetted catalyst pellets. However, the upper branch in Figure 22 illustrates that at high hydrogen to cyclohexane ratios, the catalyst in the entire reactor dries out. This leads to much higher rates and a greater temperature increase. The wet and dry branches are also influenced by phase holdup and velocities.

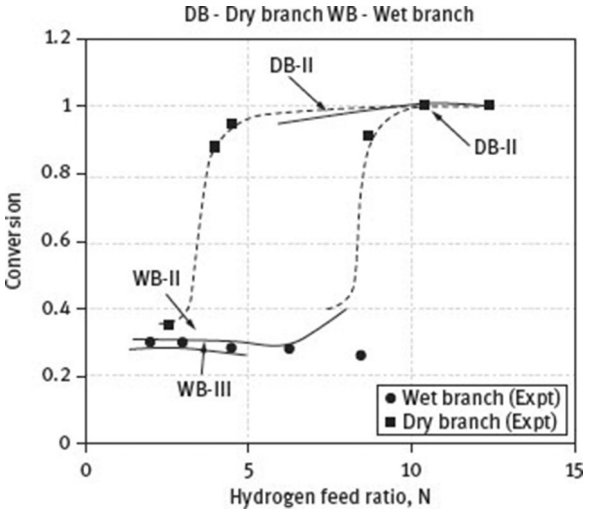

Figure 22: Multiplicity behavior of trickle bed reactors with a volatile liquid phase: conversion dependence on hydrogen to cyclohexene ratio. Reprinted from Khadilkar *et al*. © [104], with permission from Elsevier.

The application of CFD modeling to trickle bed reactors is a complex subject, owing to the discontinuous distribution of the gas and liquid, non-ideal flow behaviors including flow maldistribution, channeling and partial catalyst wetting. A very detailed review has been provided by Wang *et al*. [108]. Similar to the bubble column reactor, the typical modeling approaches may include Euler-Lagrange and Euler-Euler treatments, whilst the volume of fluid (VOF) approach is a surface tracking technique applied to a fixed Eulerian mesh when the locus of the interface between two or more immiscible fluids is of interest, such as gas-liquid interfaces encountered in the trickle bed reactor. Moving grid or fixed grids can be employed to simulate the interface. The "effective

porous medium" approach is a method of treating the trickle bed as an effective porous medium, with lumped parameters for dispersion and heat transfer, in which case modified Ergun equation or momentum balance is used to obtain the velocity field. In the "discrete particle approach", interstitial flow is modeled which accounts for the geometric complexity of the packing structure. For the trickle bed, this approach has mainly been confined to small sections or periodic regions of the bed. Various constitutive models are required to represent the momentum exchange between the phases, such as the relative permeability, slit or fundamental force balance models. Capillary pressure effect also needs to be allowed for in modeling the trickle bed reactor, whilst closure relationships are required to represent macroscopic turbulence. CFD models have been used with some success to predict liquid phase holdup, pressure drop and gas-liquid flow maldistribution in trickle beds, although prediction of flow regime transitions is very computationally intensive. Full models incorporating mass transfer and chemical reactions effect into CFD simulations has presently achieved limited success because of the very intensive computational effort that would arise from coupling the necessary conservation of species and energy equations with the CFD model. Development of improved turbulence models, efficient parallel computational algorithms to improve solution time, and validation of the CFD models using data from imaging and non-invasive monitoring of multiphase flows are some areas identified for future consideration and development.

Reports of actual industrial experience in scale up tend to be relatively scarce because of commercial intellectual property considerations, but Hickman *et al*. [109] recently reported the scale up of an industrial hydrogenation process for a proprietary hydrogenation reaction over a palladium catalyst. A laboratory scale reactor was used to screen the catalyst formulation and to obtain kinetic data for scale up. The final reactor design was scaled up from the laboratory by a factor of $\sim 3 \times 10^6$. The main problems encountered included incomplete wetting of the laboratory catalyst bed, catalyst productivity being lower than the value required for attractive economic production and difficulties associated with catalyst deactivation. The aspect ratio of the catalyst bed was increased in order to increase the liquid superficial velocity, while smaller catalyst pellets helped to avoid the problem of incomplete wetting. The issues of catalyst deactivation were studied by a range of characterization techniques upon spent catalyst samples and iron poisoning of Pd was found to be a problem leading to catalyst deactivation. Avoidance of iron contaminated feed was found to lead to a less severe deactivation rate, with sintering, fouling and leaching of Pd occurring at a slow enough rate for an economically attractive catalyst lifetime to be achieved.

3.5 Enantioselective Hydrogenation reactions

Although heterogeneous catalysts provide many advantages such as ease of separation and ability to be operated in flow reactors, homogeneous catalysts may sometimes offer enhanced activity and selectivity, particularly for synthesis of fine chemicals and pharmaceuticals, which may contain stereo, chemo and enantioselective products. Stereoisomers have the same molecular formula and sequence of bonded atoms, but differ only in the three-dimensional orientations of their atoms in space. Enantiomers consist of two stereoisomers that are mirror images of each other; they are not superim-posable, similar to one's left and right hands being the same except for their opposite orientation. The enantioselectivity of supported metal catalysts may be controlled by the addition of a very small quantity of an adsorbed chiral modifier, which is deposited on the heterogeneous catalyst surface in a special pre-treatment step before reaction. The modifier is adsorbed on the active metal surface and controls the enantioselectivity by interacting with the reactants.

Homogeneous catalysts often consist of a metal center with different ligands attached to it, which may be comprised of ions or molecules. The ligands may be designed to control the reactivity of the central atom. Owing to the potential advantages of heterogeneous and homogeneous catalysts, a relatively new field of research is the preparation and application of heterogenized metal complexes, which combine the ease of separation and recycling of heterogeneous catalysts with the high activity and selectivity of heterogeneous catalysts. Several approaches for the preparation of immobilized complexes are available, including covalent binding, adsorption, ion pair formation and entrapment or the 'ship in a bottle' approach [110]. Despite this range of immobilization procedures, it is still challenging to synthesize efficient immobilized catalysts, since the immobilized complex must maintain its activity and selectivity, be easily recovered and not leach under the reaction conditions. Augustine *et al*. [111] developed a new technique of immobilization that involves attaching catalytically active complexes to solid supports via heteropolyacids (HPA). The metal atom of the complex is attached to the support via the HPA, and thus avoids the use of the ligand for attachment, which may be prone to leaching.

The enantioselective hydrogenation of β-ketoesters to chiral β-hydroxyesters and the hydrogenation of α-ketoesters or acids to chiral α-hydroxyesters are two commonly studied enantioselective reactions [112]. In terms of homogeneous catalyst design, various chiral phosphine ligands have been developed following Wilkinson's discovery of $[RhCl(PPh_3)_3]$ as an homogeneous hydrogenation catalyst for unhindered alkenes [113]. Several

authors have then shown that the enantioselective asymmetric hydrogenation of prochiral C−C double bonds can be carried out using optically active phosphines as ligands in complexes of rhodium [114]. The production of enantiopure products is of paramount importance for applications such as pharmaceuticals. Baiker [115] asserted that research in enantioselective catalysis has been driven by the well-known fact that the incorrect enantiomer of a chiral product may have negative side effects that outweigh the beneficial value of the correct enantiomer, the birth defects caused by the drug thalidomide being an example. Currently the production of enantiopure compounds is carried out at the industrial scale using batch processing. However, the replacement of batch processes with continuous would be natural step forward as the demand for increased production volumes of fine chemicals is expected to increase [116]. Some examples of large scale production of fine chemicals include the painkiller Ibuprofen (10 000 tonnes/annum), sweetener S,S-aspartame (14 000 t/a) and herbicide (R)-mecropol (14 000 t/a).

Only a few examples of the application of continuous processes for enantioselective catalysis are reported in the literature. Kunzle *et al*. [117] reported the continuous enantioselective hydrogenations of some substrates including ethyl pyruvate, keto-pantolactone and 1-phenyl-1,2-propanedione over cinchona modified Pt/alumina catalysts. However, a drawback of their approach was that a continuous small top-up feed of cinchona modifier was required to be added to the inlet stream to maintain enantioselectivity. The catalyst used was in the form of very small particles, which could lead to a higher pressure drop in the trickle bed; a higher cinchona alkaloid/substrate ratio was required compared with batch processes [118]. In order to solve the problem of high pressure drop across the catalyst bed, Toukoniitty *et al*. [116] used a knitted silica fiber support material impregnated with platinum for the enantioselective hydrogenation of 1-phenyl-1,2-propanediol in a fixed bed reactor. Although the initial enantioselectivity of 23% was very low, it increased to a steady state value of 57 %, with continuous feed of modifier to the reactor being necessary. Al Herz *et al*. [119] studied the catalytic hydrogenation of dimethyl itaconate in a laboratory scale trickle bed reactor with a liquid feed recycle. The enantioselectivity or enantiomeric excess (ee) of the reaction was determined as (S − R)/(S + R), where S and R refer to the product enantiomers. A catalyst complex [Rh((R,R)-Me-DuPhos)(COD)]BF_4 was used in an immobilized form by attachment to alumina support powder or pellets using phostungstic acid (PTA) as an anchoring agent. Preliminary experiments were carried out in a shake flask to determine the kinetics: substrate to catalyst molar ratio 60, atmospheric pressure, room temperature (293.15 K), H_2 flow rate of 100 ml min^{-1}, agitation speed of 200 rpm, whereupon a turnover frequency of 50 h^{-1} was obtained with the powdered alumina support and enantioselectivity 96 %. The reaction rate data were fitted using Osborne-Wilkinson kinetics [120]. The rate determining step can be one of two possible paths: (1) attack of the uncomplexed olefin on the dihydro-complex at the vacant site giving a transition state in which both hydrogen and olefin are bound to the metal; and (2) attack of molecular hydrogen on the olefin complex leading to the same transition state. The rate may be expressed as:

$$R = \frac{d[S]}{dt} = \frac{(k'K_1 + k''K_2)\, p\, [S]\, [A]}{1 + K_1 p + K_2 [S]}, \tag{32}$$

where k' and k'' are rate constants, K_1 and K_2 are equilibrium constants [S] and [A] are concentrations of substrate and catalyst respectively, p is the concentration of hydrogen in the solution. The constants were fitted using experimental data, where it was shown the value of K_2 is much greater than K_1, indicating that the formation of the olefin complex is favored. The reaction in the fixed bed was carried out in the trickle flow regime using a laboratory scale set up with a bed of 6 mm diameter and a total height of 100 mm. Gas and liquid flowrates were found to have a noticeable effect upon the initial reaction rate and enantioselectivity, and optimization of flowrates was studied. The liquid flowrate was found to have the stronger effect, being directly proportional to the wetting efficiency of the catalyst bed and rate of mass transfer of hydrogen from the bulk liquid to the catalyst surface. Optimal conditions were found to be: substrate/catalyst molar ratio of 223, atmospheric pressure, room temperature (293.15 K), 100 ml min^{-1} gas flowrate, 20 ml min^{-1} liquid flowrate, at which a conversion of DMI of 99 % and enantioselectivity of 99.9 % were achieved. The results showed some promising behavior for possible scale up of enantioselective reactions for application in the trickle bed; however, for truly continuous operation, conversion per pass of reactants through the bed would need to be increased instead of the batch recycle mode.

3.6 Industrial applications in heavy oil upgrading

Trickle bed reactors have traditionally been used in petroleum refining processes such as hydrocracking, hydrodesulphurization and hydrodearomatization, for example. However, with the decline in the reserves of light oils, attention is switching to alternative energy sources such as heavy crude oil and bitumen, for short

to medium-term energy needs. Heavy oils are asphaltic and dense; viscous oils have an API gravity between 10 and 20 °API. The American Petroleum Institute gravity or API gravity is a measure of how heavy or light a petroleum liquid is compared to water, with higher values representing lighter oils. Bitumens or oil sands have similar attributes to heavy oil but are even more viscous and dense, with viscosities usually greater than 10 000 cP and API gravity less than 10 °API. Such oils require more energy intensive operations for their production, upgrading and transportation. Due to the potentially higher cost of such extraction methods, a range of Enhanced Oil Recovery (EOR) techniques have been proposed and developed to try to extract as much of the oil in place as possible. These include miscible displacement with gases such as CO_2, flooding with chemicals, surfactants or polymers, microbial enhanced recovery methods and thermal methods [121]. The thermal methods encompass technologies requiring steam injection, such as steam flooding, cyclic steam stimulation and steam assisted gravity drainage (SAGD). Alternatively, *in situ* combustion can be used, which works by burning a small fraction of the oil by injecting air into the reservoir in order to enable flow of the remaining oil and enhance the oil production rate. This is normally achieved by the injection of an oxidizing gas such as air. 'Toe-to-heel' Air Injection (THAI) combines ISC with a horizontal production well, as shown in Figure 23. The well is initially steamed to raise its temperature; thereafter, air is injected to ignite the *in situ* combustion process. The flame front moves gradually along the horizontal well from the 'toe' position to the 'heel'. The process offers good scope for control of the combustion since a coke layer forms as the combustion front passes, preventing the bypass of gas over the heavy oil layer.Up to 80–85%recovery of the oil in place may be possible, which is significantly higher than alternative techniques. A catalytic add-on to the process was also developed, termed CAPRI, which involves the packing of an annular layer of refinery hydrotreatment catalyst surrounding the horizontal well: in effect, the well becomes the reactor with *in situ* upgrading taking place. The upgrading reactions occurring in the THAI process are thought to occur in the Mobile Oil Zone (MOZ). The reactions taking place include (i) carbon rejection reactions as a result of thermal cracking, and (ii) hydrogen addition when the already lighter, cracked components contact the hydrotreating catalyst in the annular layer (CAPRI) surrounding the producer well. Field trials of THAI have been carried out by Petrobank at their White Sands pilot project in 2006, at Christina Lake, Alberta, Canada. Maximum gross oil production per well pair was reported as 2000 barrels/day with a bitumen cut of around 55 %. The produced oil was found to be partially upgraded in the range of 10.6 to 16.1 °API. The THAI-CAPRI upgrading mechanism can simply be represented by the following equations:

Thermal cracking (Pyrolysis):

$$\text{Heavy residue} \rightarrow \text{Light oil} + \text{coke}$$

Oxidation of coke (high temperature oxidation):

$$\text{Coke} + O_2 \rightarrow CO + CO_2 + H_2O$$

Oxidation of heavy residue:

$$\text{Heavy residue} + O_2 \rightarrow CO + CO_2 + H_2O$$

Carbon rejection:

$$CH_x \rightarrow CH_{x1} + C \qquad (x_1 > x)$$

Hydrogen addition:

$$CH_x + H_2 \rightarrow CH_{x1} \qquad (x_1 > x)$$

Upgrading of heavy oil/natural bitumen is a very complex process, so the hydrogen responsible for the upgrading of the THAI-CAPRI produced oil is thought to be formed due to the water gas shift reaction, and is represented with the following simple equations:

Gasification of hydrocarbon:

$$CH_x \rightarrow C + \frac{x}{2}H_2$$
$$C + H_2O\,(\text{steam}) \rightarrow CO + H_2$$
$$C + CO_2 \rightarrow CO$$

Water-gas shift:

$$CO + H_2O \rightarrow CO + H_2$$

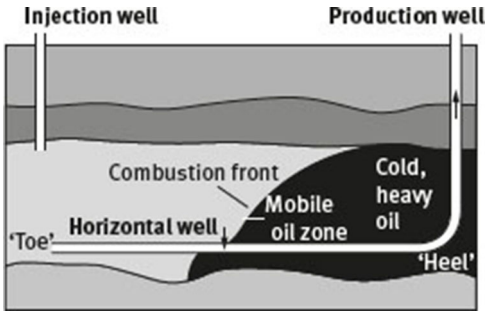

Figure 23: Schematic diagram showing heavy oil recovery using Toe-to-Heel Air Injection method (THAI). Reprinted from Shah *et al*. © [121], with permission from Royal Society of Chemistry.

It can be observed that coke is produced by the reactions, which may lead to possible deactivation of the catalyst. Therefore Shah *et al*. [122] made a laboratory-based study of the optimization of process conditions for *in situ* heavy oil and bitumen recovery using the THAI-CAPRI process. A rig was developed consisting of two microreactors for the purpose of simulating *in situ* oil upgrading conditions in well. Each reactor contains a fixed bed of catalyst to represent a cylindrical core of 10.2 mm diameter taken in a radial direction through the annular layer of catalyst packed around the producer well. Associated equipment includes a gas supply system, trace heating, furnace, temperature control system and gas-liquid separator. Experiments were carried out on a feed oil supplied from the THAI trials at the White Sands field by Petrobank. The microreactors were packed with 10 g of catalyst samples such as CoMo, NiMo and ZnO/CuO. An oil flow of 1ml/min and gas flow of 0.5 l/min were used under different temperatures, pressures and gas environments. Selected experiments were carried out using a gas mixture representative of the combustion gases from the THAI process, namely 80 % N_2, 13% CO_2, 3% CO and 4% CH_4. Other experiments were carried out under a flow of nitrogen. It was found that temperature has a strong effect upon the upgrading occurring and catalyst lifetime. Operation at 500 °C and 20 bar led to an average of 6.1 °API upgrading of THAI feed oil to 18.9 °API, however catalyst lifetime was limited to just 1.5 hours. Reduction of the temperature to 420 °C was found to lead to a lower extent of upgrading of an average of 1.6 °API, and sometimes up to 3 °API, but catalyst lifetime was considerably extended up to 77.5 hours. The process was less sensitive to changes in gas-flow rate and pressure. Substantial catalyst deactivation occurred in the first few hours of the reaction, such that the pore space became blocked. In order to try to mitigate the effects of coke deposition, [123] studied the effect of guard bed and hydrogen upon the upgrading process. A guard bed involves the packing of inert porous particles above the catalyst in order to adsorb or filter coke precursors from the feed before they reach the catalyst. Hart *et al*. [123] used a layer of activated carbon particles for this purpose, over the CoMo catalyst. Furthermore, the addition of hydrogen was studied to augment catalytic hydroconversion and hydrocracking reactions in order to achieve a higher level of upgrading than would be achieved with inert gases. It was found that depending on the upgrading temperature, the viscosity of the produced oil reduced significantly by 42–82 % and API gravity increased by ~2 to 7°API relative to the feedstock of 0.49 Pa s and 13°API, respectively. Conversely, the use of hydrogen further increased the API gravity by 2 °API and the viscosity by 5.3 %. Notably, the coke content of the catalyst reduced from 57.3wt% in nitrogen to 34.8 wt % in hydrogen atmosphere. The use of a guard bed increased the API gravity of the produced oil by a further 2° and reduced the viscosity by an average of 8.5 % further than achieved with the active HDS catalyst CoMo/alumina. Catalytic hydrocracking is thought to involve the breaking of larger molecules to give fragmented free radicals, which then react with hydrogen radicals in order to stabilize the hydrocarbon chains and terminate the reaction. In the absence of hydrogen, the active chains keep reacting with each other, resulting in the formation of higher molecular weight compounds by polymerization, increased coke formation and adverse impact of viscosity and API upgrading of the produced oil.

4 Structured monolith reactors

Monolithic catalysts were initially developed for use in automotive exhaust emission control, but during the past 10–15 years increasing interest has occurred in their application to a more diverse range of areas in the chemical and allied industries [57]. Structured honeycomb monolith catalyst supports are usually comprised of parallel, usually straight capillary channels upon which the catalyst is coated within a wash coat layer of

porous material. In the field of energy, monolith reactors have been applied for hydrogen production from steam reforming [124], water gas shift reaction [125], methanation of carbon dioxide to produce methanol [126] and manufacture of synthetic fuels using Fischer-Tropsch synthesis [127]. The purification of air or water by monolithic catalysts has been studied [128, 129] as well as the catalytic reduction of pollutants such as NO_x from stationary sources [130, 131]. Although originally applied to gas phase systems, new applications of monoliths in three-phase gas-liquid-solid applications have been considered [132, 133]. Reaction systems of interest include hydrogenations, for example of 2-butyne-1,4-diol [134], nitrobenzoic acid [135], α-methyl styrene [136], benzaldehyde [137], pyrolysis gasoline [138] and oxidations such as of glycerol [139], glucose [140] and ethanol [141]. However, one of the few known scaled up industrial applications is in the production of hydrogen peroxide [142].

The monolith reactor has the advantage that intensified performance can be achieved with much lower power inputs than some alternative process intensification devices. Key to this enhancement of performance is the length scales over which reaction and mixing occur in the monolith reactor. Although a range of flow patterns may occur within the channel, one of the most desirable regimes for enhanced mass transfer is 'Taylor flow' or bubble train flow, in which liquid slugs separated by gas bubbles flow along each channel. This creates a thin film of liquid at the sides of the gas bubbles in contact with the catalyst coating on the channel wall, the thickness of which may range from 5–50 μm for fluids of low viscosity [143]. Typically, the channel side length in monoliths is of the order of 1–2 mm and optimum washcoat thickness is of the order 70 μm, for example in the case of Syngas production [144]. These scales mean that the momentum balance and bulk mass transfer occur over the characteristic length of the channel diameter of the order of millimeters, whilst diffusion across the liquid film and into the washcoat occurs over distances of the order of tens of microns [145]. Reaction occurs at catalytic sites in pores of the order of tens of nanometers, within the washcoat. These small length scales can be contrasted with the much larger sizes in traditional reactors such as fixed and trickle beds, which utilize extrudate pellets of several millimeters length within reactors on the scale of several meters. By minimizing the transport and diffusion distances, utilizing a thin catalyst washcoat, enhancing mixing within the channels and bringing the reactants together in intimate contact, monolith reactors represent an advantageous technology for process intensification. They can lead to improved reactant conversion, selectivity towards desirable products and improved process safety [132].

4.1 Flow patterns in the single capillary

4.1.1 Flow regimes

The performance of the monolith reactor as a high-intensity mass transfer device is very dependent upon the flow pattern of gas and liquid within the monolith channels. Therefore, it is important to understand the conditions under which certain flow patterns occur and to be able to predict mass transfer parameters for these flow regimes. In some earlier studies, Satterfield and Ozel [146] showed that the flow regimes are strongly influenced by the wettability between the liquid and the capillary wall as well as the surface tension between the liquid and gas phases. A wealth of literature exists for gas-liquid two-phase flows in pipes and channels, for example Taitel *et al*. [147] presented a comprehensive model for flow pattern transitions in large diameter tubes for vertical upflow. However, such studies were not representative of the correct length scales of monolith channels with diameters of 1–2 mm. Thulasidas *et al*. [143] carried out some of the first detailed hydrodynamic studies at scales relevant to monolith channels operating in upflow mode and determined the main mass transfer parameters, such as bubble size, shape, velocity and volume fraction of gas inside capillaries of circular or square cross section on the basis of the superficial flow rates of gas and liquid in the feed. However, monolith reactors such as the CDCR operate in downflow mode and later studies of downflow in monolith channels were carried out by Tsoligkas *et al*. [148] for 1.5–2mm square glass capillaries, which represent a single channel in a monolith reactor. Using a high-speed camera, five flow patterns and three transitional flow patterns were observed as shown in Figure 24. The regimes most worthy of note are (a) annular Flow, (c) Taylor flow, also known as regular slug or bubble-train flow, (e) bubbly flow (h) churn flow, with the others representing transitional regimes. Flow regime maps were determined for air-water and air-water/isopropanol mixtures, which may be used to guide the selection of gas and liquid velocities in order to achieve the desired flow regime within the monolith. Taylor flow is a desirable regime in which to operate in order to maximize the transfer of a gas such as hydrogen to the catalyst surface within the three-phase reactor, owing to the thin liquid films formed at the sides of the gas bubble.

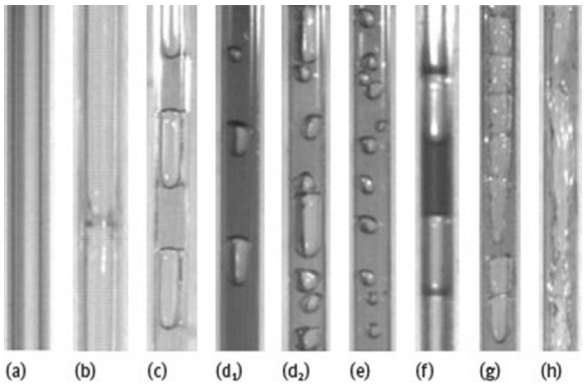

Figure 24: Flow patterns in a square capillary tube for vertical down-flow. (a) annular flow; (b) slug– annular flow; (c) Taylor (regular slug) flow; (d) slug–bubbly flow; (e) bubbly flow; (f) irregular slug flow; (g) slug–churn flow; and (h) churn flow. Reprinted from Tsoligkas *et al*. © [148], with permission of Elsevier.

4.1.2 Mixing and mass transfer

In order to design and optimize the monolith reactor in three-phase operation, it is necessary to understand the different modes of mass transfer which may be (1) gas-liquid-solid (GS) via the liquid film, (2) gas-liquid (GL) via the gas bubble caps and (3) liquid-solid (LS) within the liquid slugs. In this section, flow studies of the liquid slugs are reviewed, followed by the mass transfer characteristics of the three-phase monolith reactor.

4.1.3 Recirculation in liquid slugs

Within the liquid slugs that occur in Taylor flow, mass transfer processes (2) GL and (3) LS as mentioned above occur and therefore it is important to understand the mechanisms of mixing which assist this mass transfer. Thulasidas *et al*. [143] used Particle Image Velocimetry (PIV) to study the velocity distributions in liquid slugs in Taylor flow operated in 'upflow' mode, and showed that recirculating patterns occur with a high degree of mixing. The detailed behavior is a function of the capillary number,

where

$$Ca = \frac{\mu V}{\sigma}. \tag{33}$$

Depending on the capillary number of the flow, counter rotating vortices or a complete bypass flow inside the liquid slug were observed. Such recirculation patterns can play an important role in transporting dissolved gas from the bubble cap to the catalyst coated upon the channel walls. Tsoligkas *et al*. [148] also used PIV to study flow in liquid slugs, but in downflow mode. They found that short slugs (slug length less than the tube hydraulic diameter) led to a relatively flat velocity profile, where the axial velocity is only a function of the position in the tube cross-section, as shown in Figure 25. By contrast, in long slugs the axial velocity component depends upon both the axial position in the tube and the tube cross-section. Parabolic velocity profiles are approximated for $V_{max}/V_b \approx 1.1-1.7$. Significant differences from upflow operation were observed with upflow recirculation times being three times faster than downflow; this has implications for the models used to predict mass transfer and residence time distribution.

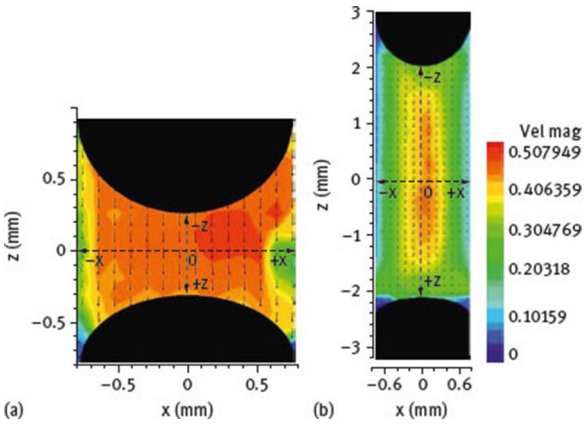

Figure 25: Flow fields within the liquid slugs determined by PIV in the $W = 1.5$ mm tube for (a) $L_S < D_c$, 30 % v/v isopropanol/water–air mixture, $C_a = 0.008$, $V_{GS} = 0.384$ m s^{-1}, $V_{LS} = 0.111$ m s^{-1}, $V_B = 0.576$ m s^{-1}; (b) $L_S > D_c$, water–air mixture, $C_a = 0.0287$, $V_{GS} = 0.209$ m s^{-1}, $V_{LS} = 0.106$ m s^{-1}, $V_B = 0.343$ m s^{-1}. Units of velocity are m s^{-1}. Reprinted from Tsoligkas *et al*. © [148], with permission of Elsevier.

4.1.4 Mass transfer processes

A detailed analysis of the mass transfer steps involved in Taylor flow within the monolith reactor has been given by Kreutzer *et al*. [133], and is summarized in this section. The three mass transfer modes of steps (1)–(3) from above may be combined, with the (2) GL and (3) LS steps considered as resistances in series; they are in parallel with respect to (1) GS mass transfer. For the overall mass transfer, the following expression can be used:

$$k_{OV}a = k_{GS}a_{GS} + \left(\frac{1}{k_{GL}a_{GL}} + \frac{1}{k_{LS}a_{LS}}\right)^{-1}. \tag{34}$$

The individual mass transfer coefficients and areas are determined as:

$$k_{GS} = \frac{(\mathscr{D})}{\delta}, \tag{35}$$

$$a_{GS} = \frac{1\,(1-\varepsilon_L)}{D_c}, \tag{36}$$

$$k_{GL}a_{GL} = \frac{0.133U_{TP}^{1.2}}{L_{slug}^{0.5}}, \tag{37}$$

$$k_{LS}a_{LS} = \frac{(\mathscr{D})}{\delta}\frac{4\varepsilon_L}{D_c}. \tag{38}$$

In Eqs. (35) and (38), the film thickness δ is an important parameter, which strongly influences the rate of mass transfer. The film thickness is influenced by the Capillary number and thus from Eq. (33) it can be observed that the unit cell velocity, as well as the viscosity and surface tension of the fluid have a strong effect upon the mass transfer rates in the reactor.

4.2 Applications in hydrogenation reactions

Monolith reactors have been studied for an increasing range of applications in three-phase reactions, and are particularly effective for hydrogenation, dehydrogenation and oxidation reactions [137, 149, 150]. However, rational evaluation of the performance of such reactors must be made on the basis of a comparison with other traditional reactor designs. Fishwick *et al*. [17] made a comparison of selective hydrogenations in the monolith CDC, stirred tank and trickle bed reactors with configurations shown in Figure 26. The selective hydrogenation of 2-butyne-1,4-diol (B3D) was used as the test reaction, which has the reaction scheme shown in Figure 6. This is a consecutive reaction, in which the alkene intermediate, 2-butene-1,4-diol (B2D) is an important chemical in the manufacture of vitamins, pharmaceuticals and insecticides. The fully hydrogenated product 2-butane-1,4-diol (B1D) is a raw material used in the polymer industry and manufacture of tetrahydrofuran. Five reactors were compared, which included a stirred tank, trickle bed reactor, single capillary reactor, 5 cm diameter monolith CDCR and 10 cm diameter monolith CDCR. All of the reactors were operated at a pressure of 200 kPa, except the single capillary which was operated at 100 kPa and a temperature of 55 °C was used in each case. Industrial Pd/Al_2O_3 catalysts, supplied by Johnson Matthey, were tested, which included a powdered 1% γ-Pd/Al_2O_3 (stirred tank), 0.5 % Pd/Al_2O_3 pellet (trickle bed) and a washcoated Pd/α-Al_2O_3 monolith. Each catalyst was typical of the industrial catalyst used in that type of reactor, and in order to facilitate a comparison of the different reactors, rates were reported as normalized per gram of palladium. Solvents used in the reaction included water, 2-propanol and a 30% v/v mixture of 2-propanol in water.

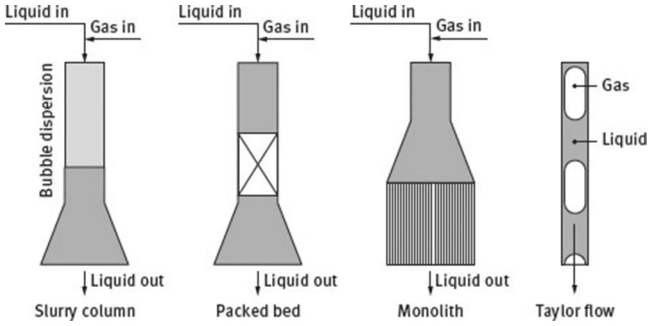

Figure 26: Schematic diagram illustrating the CSTR, packed bed, single capillary, 5 cm diameter monolith and 10 cm diameter monolith operation in the CDCR.

Table 4 displays the initial rate and selectivity towards B2D at B3D conversions of 90 % and 100 % for a range of different solvent compositions and reactor types. Selectivity, *S*, is defined at the mole fraction of the intermediate (B2D) in the total number of moles of product. From Table 4 it can be observed that the B2D selectivity is generally very high, but that the structured monoliths lead to higher selectivities than both the stirred tank and trickle beds, regardless of which solvent is used. High selectivity towards B2D was thought to be associated with effective mass transfer of hydrogen to the catalyst surface. This ensures that the active sites are sufficiently populated with hydrogen so that hydrogenation occurs in preference to the formation of side products by reactions that do not consume hydrogen, for example 4-hydroxybutanal, 2-buten-1-ol or the derivatives of these products shown in Figure 6. However, if the concentration of hydrogen at the surface is too high, it could lead to over-hydrogenation of the alkene to produce the alkane and thus decrease the selectivity. Also a close approximation to plug flow, as expected in the monoliths, could reduce the amount of time that the intermediate alkene spends in contact with the catalyst and thus decrease the extent of over-hydrogenation to form the alkane. In the monoliths, the mass transfer coefficients of hydrogen at both the gas-liquid and liquid-solid interfaces were substantially higher than in the stirred tank and trickle bed, which would be expected to lead to better availability of hydrogen at the catalyst surface and thus increase selectivity towards the hydrogenation products, rather than promoting side reactions. The performance of the monolith was also found to be dependent upon the hydrodynamic mode of operation, that is whether the gas bubble dispersion is allowed to penetrate in to the monolith channels, such that Taylor flow occurs in the channels, or liquid is pre-saturated with hydrogen by controlling the bubble dispersion to remain in the upper part of the column. Higher mass transfer rates were observed when the monolith is operated in two-phase flow.

Table 4 Initial reaction rates and selectivity towards cis-2-butene-1,4-diol for CDC monolith, stirred tank (STR) and trickle bed reactors (TBR). Reprinted from Fishwick *et al*. © [17], with permission of Elsevier.

Solvent	**Reactor**	**Initial Rate** $\left[\mathrm{mol\,s^{-1}\,g_{Pd}^{-1}}\right]$	**Selectivity *S***	
(90% conversion)	**(100% conversion)**			
Water	5 cm monolith	0.186×10^{-3}	1.00	1.00
	10 cm monolith	0.186×10^{-3}	1.00	0.96
	STR	0.264×10^{-3}	0.99	0.93
TBR	0.033×10^{-3}	0.87	0.86	
30%v/v 2-Propanol	5 cm monolith	0.206×10^{-3}	1.00	1.00
in water (M)	10 cm monolith	0.206×10^{-3}	1.00	1.00
	STR	0.319×10^{-3}	1.00	0.95
TBR	0.330×10^{-3}	0.93	0.90	
2-Propanol	5 cm monolith	0.268×10^{-3}	0.99	0.90
STR	0.522×10^{-3}	0.97	0.87	

Referring again to Table 4, for the use of the mixed water/2-propanol solvent, complete selectivity towards the alkene is achieved without the requirement of using dopants or poisoning the catalyst with addition of bases. The effect of a solvent type upon the reaction behavior could be partly explained in terms of higher hydrogen solubility in 2-propanol compared with water, leading to higher rate of hydrogenation. Also, in mixtures of 2-propanol, the bubble size is influenced by the solvent composition, which in turn affects the gas-liquid interfacial area. Of the three solvents studied, the smallest bubbles observed by a video-microscope-computer system occur for a mixture of 2-propanol in water mixture; therefore, a higher gas-liquid interfacial area is observed [9]. These studies show that suitable selection of reactor type, operating conditions and solvent can

lead to improved selectivity towards the desirable product, therefore decreasing the production of undesirable waste.

In some cases, structured reactors open up new reaction routes or make reactions feasible that would otherwise have low rates and selectivities in the autoclave. The oxidation of glycerol, a by-product of the biodiesel industry, can be used to produce a range of useful products. Glycerol is available from sustainable sources, but traditional oxidation processes used in industry sometimes involve environmentally unfriendly reagents such as dichromate, permanganate, manganese and peroxides [151]. Hutchings *et al*. [58] has shown that gold catalysts are active for selective oxidation reactions, using molecular oxygen as the oxidizing agent and is very selective for the oxidation of glycerol to glycerate. The addition of base, such as sodium hydroxide, is required to accelerate the rate-limiting deprotonation step. Pollington *et al*. [139] studied the selective oxidation of glycerol in several multiphase reactors. The flow reactors consisted of a laboratory scale loop system operated in batch-recycle mode. The catalyst or support used included an Au/C catalyzed monolith or a cordierite monolith without metal coating, in which case the Au/C catalyst powder was placed in the feed tank with the liquid such that slurry flowed through the uncoated monolith during operation, denoted as a meso-structured slurry bubble column (MSSBC). Comparisons were made with studies of the same reaction in an autoclave. It was observed that the highest rate occurred in the MSSCB (109–201 mmol glycerol s^{-1} m^{-3} bar^{-1}), followed by the catalyst coated monolith (36–65 mmol glycerol s^{-1} m^{-3} bar^{-1}), and lastly the stirred reactor (4 mmol glycerol s^{-1} m^{-3} bar^{-1}). Selectivity towards glyceric acid was 100 % for the monolith and autoclave, but in the MSSBC the production of dihydroxyacetone and glyceric acid was approximately equal, thus selectivity towards glyceric acid was in the range 47–54 %. The lower selectivity in the MSSBC was attributed to better oxygen availability than the monolith and autoclave reactors. The study illustrated the benefits of structuring catalysts, where the monolith gave rise to enhanced reaction rates while maintaining high selectivity, which arises from enhanced mass transfer via thin liquid films when the gas-liquid mixture flows through the channels of the monolith catalyst.

5 Conclusions

This chapter has reviewed research covering a range of three-phase reactors including stirred tanks, bubble columns, trickle beds and monolith reactors. Case studies have been described to illustrate the application of these reactors in a range of hydrogenation and oxidation reactions from the laboratory to industrial scale operations. The interplay between hydrodynamics, mass transfer, mixing and reaction kinetics has been highlighted in the discussion. The selection of a suitable catalyst must also be accompanied by analysis of transport processes in the reactor to determine the limiting step, and issues concerning catalyst deactivation must also be understood. The development of non-invasive imaging techniques such as PEPT, CARPT, MRI and PIV has led to improved understanding of the mixing processes occurring in a range of three-phase reactors. Results from such experimental studies have been used to validate CFD models of three-phase flows of increasing complexity. The combination of these tools has led to increased confidence for scale up of processes for industrial application.

Acknowledgments

This article is also available in: Saha, Catalytic Reactors. De Gruyter (2015), isbn 978-3-11-033296-4.

References

[1] Biardi G, Baldi G. Three-phase catalytic reactors. Catal Today 1999, 52, 223–234.
[2] Winterbottom JM, King MB. Reactor design for chemical engineers. Cheltenham, UK, Stanley Thornes, 1999.
[3] Ramachandran PA, Chaudhari RV. Three-phase catalytic reactors. New York, Gordon and Breach Science Publishers, 1983.
[4] Gianetto A, Silveston PL, Baldi G. Multiphase chemical reactors: theory, design, scale up. Washington; Berlin; New York, Hemisphere Pub. Corp. ; Distribution outside North America, Springer-Verlag, 1986.
[5] Fogler HS. Elements of chemical reaction engineering. Upper Saddle River, N.J Prentice Hall PTR, 1999.
[6] Markopoulos J, Christofi C, Katsinaris I. Mass transfer coefficients in mechanically agitated gas-liquid contactors. Chem Eng Technol 2007, 30, 829–834.
[7] Kawase Y, Araki T, Shimizu K, Miura H. Gas-liquid mass transfer in three-phase stirred tank reactors: Newtonian and non-Newtonian fluids. Can J Chem Eng 1997, 75, 1159–1164.
[8] Rajadhyaksha RA, Karwa SL. Solvent effects in catalytic-hydrogenation. Chem Eng Sci 1986, 41, 1765–1770.

[9] Hu B, Fishwick RP, Pacek AW, *et al.* Simultaneous measurement of in situ bubble size and reaction rates with a heterogeneous catalytic hydrogenation reaction. Chem Eng Sci 2007, 62, 5392–5396.
[10] Hu B, Pacek AW, Stitt EH, Nienow AW. Bubble sizes in agitated air-alcohol systems with and without particles: Turbulent and transitional flow. Chem Eng Sci 2005, 60, 6371–6377.
[11] Hu BJ, Nienow AW, Stitt EH, Pacek AW. Bubble sizes in agitated solvent/reactant mixtures used in heterogeneous catalytic hydrogenation of 2-butyne-1,4-diol. Chem Eng Sci 2006, 61, 6765–6774.
[12] Fishwick RP, Winterbottom JM, Parker DJ, Fan XF, Stitt EH. Hydrodynamic measurements of up- and down-pumping pitched-blade turbines in gassed, agitated vessels, using positron emission particle tracking. Ind Eng Chem Res 2005, 44, 6371–6380.
[13] Mahouast M, Cognet G, David R. 2-Component LDV measurements in a stirred tank. Aiche Journal 1989, 35, 1770–1778.
[14] Sheng J, Meng H, Fox RO. Validation of CFD simulations of a stirred tank using particle image velocimetry data. Can J Chem Eng 1998, 76, 611–625.
[15] Devanathan N, Moslemian D, Dudukovic MP. Flow mapping in bubble-columns using CARPT. Chem Eng Sci 1990, 45, 2285–2291.
[16] Leadbeater TW, Parker DJ. A modular positron camera for the study of industrial processes. Nuclear Instruments & Methods in Physics Research Section a-Accelerators Spectrometers Detectors and Associated Equipment 2011, 652, 646–649.
[17] Fishwick RP, Natividad R, Kulkarni R, *et al.* Selective hydrogenation reactions: A comparative study of monolith CDC, stirred tank and trickle bed reactors. Catal Today 2007, 128, 108–114.
[18] Wang M, Dorward A, Vlaev D, Mann R. Measurements of gas-liquid mixing in a stirred vessel using electrical resistance tomography (ERT). Chemical Engineering Journal 2000, 77, 93–98.
[19] Mills PL, Chaudhari RV. Reaction engineering of emerging oxidation processes. Catal Today 1999, 48, 17–29.
[20] Froment GF, Bischoff KB. Chemical reactor analysis and design. New York, Wiley, 1990.
[21] Mills PL, Chaudhari RV. Multiphase catalytic reactor engineering and design for pharmaceuticals and fine chemicals. Catal Today 1997, 37, 367–404.
[22] Brahme PH, Doraiswamy LK. Modeling of a slurry reaction - hydrogenation of glucose on raney-nickel. Industrial & Engineering Chemistry Process Design and Development 1976, 15, 130–137.
[23] Chaudhari RV, Mills PL. Multiphase catalysis and reaction engineering for emerging pharmaceutical processes. Chem Eng Sci 2004, 59, 5337–5344.
[24] Irandoust S, Andersson B. Mass-transfer and liquid-phase reactions in a segmented 2-phase flow monolithic catalyst reactor. Chem Eng Sci 1988, 43, 1983–1988.
[25] Gupte SP, Chaudhari RV. Carbonylation of 2,4-dinitrotoluene using homogeneous Pd and Rh complex catalysts. Journal of Molecular Catalysis 1984, 24, 197–210.
[26] Bond GC, Wells PB. Hydrogenation of acetylene .2. Reaction of acetylene with hydrogen catalyzed by alumina-supported palladium. J Catal 1966, 5, 65–73.
[27] Bond GC, Wells PB. Hydrogenation of acetylene .3. Reaction of acetylene with hydrogen catalyzed by alumina-supported rhodium and iridium. J Catal 1966, 5, 419–427.
[28] Freidlin LK, Kaup, II. Selectivity and stereospecificity in hydrogenation of acetylene hydrocarbons on metal catalysts. Doklady Akademii Nauk Sssr 1963, 152, 1383 ff.
[29] Arafa EA, Webb G. A C-14 radiotracer study of the hydrogenation of ethyne over EUROPT-1. Catal Today 1993, 17, 411–418.
[30] Margitfalvi J, Guczi L, Weiss AH. Reaction routes for hydrogenation of acetylene-ethylene mixtures using a double labeling method. React Kinet Catal Lett 1980, 15, 475–479.
[31] Guczi L, Tetenyi P. Some new aspects of mechanism of hydrogen exchange and hydrogenation reaction over metal catalyst .2. Hydrogenation of ethylene by tritiated hydrogen on ni catalyst. Zeitschrift Fur Physikalische Chemie-Leipzig 1968, 237, 356 ff.
[32] Borodzinski A, Cybulski A. The kinetic model of hydrogenation of acetylene-ethylene mixtures over palladium surface covered by carbonaceous deposits. Appl Catal A-Gen 2000, 198, 51– 66.
[33] Duca D, Arena F, Parmaliana A, Deganello G. Hydrogenation of acetylene in ethylene rich feedstocks: Comparison between palladium catalysts supported on pumice and alumina. Appl Catal A-Gen 1998, 172, 207–216.
[34] Kaltchev M, Stacchiola D, Molero H, Wu G, Blumenfeld A, Tysoe WT. On the reaction pathway for the formation of benzene from acetylene catalyzed by palladium. Catalysis Letters 1999, 60, 11–14.
[35] Stacchiola D, Calaza F, Zheng T, Tysoe WI. Hydrocarbon conversion on palladium catalysts. Journal of Molecular Catalysis a-Chemical 2005, 228, 35–45.
[36] Jackson SD, Hamilton CA, Kelly GJ, de Bruin D. The hydrogenation of C-5 alkynes over palladium catalysts. React Kinet Catal Lett 2001, 73, 77–82.
[37] Boitiaux JP, Cosyns J, Robert E. Hydrogenation of unsaturated-hydrocarbons in liquid-phase on palladium, platinum and rhodium catalysts .3. Quantitative selectivity ranking of platinum, palladium and rhodium in the hydrogenation of 1-butene, 1,3-butadiene and 1-butyne using a single reaction scheme. Applied Catalysis 1987, 35, 193–209.
[38] Boitiaux JP, Cosyns J, Vasudevan S. Hydrogenation of highly unsaturated-hydrocarbons over highly dispersed palladium catalyst .1. Behavior of small metal particles. Applied Catalysis 1983, 6, 41–51.
[39] Boitiaux JP, Cosyns J, Derrien M, Leger G. Newest hydrogenation catalysts. Hydrocarbon Processing 1985, 64, 51–59.
[40] Hamilton CA, Jackson SD, Kelly GJ, Spence R, de Bruin D. Competitive reactions in alkyne hydrogenation. Appl Catal A-Gen 2002, 237, 201–209.
[41] Teschner D, Vass E, Havecker M, *et al.* Alkyne hydrogenation over Pd catalysts: A new paradigm. J Catal 2006, 242, 26–37.
[42] Canning AS, Jackson SD, Mitchell S. Identification, by selective poisoning, of active sites on Ni/Al2O3 for hydrogenation and isomerisation of cis-2-pentenenitrile. Catal Today 2006, 114, 372–376.
[43] Bennett JA, Fishwick RP, Spence R, *et al.* Hydrogenation of 2-pentyne over Pd/Al2O3 catalysts: Effect of operating variables and solvent selection. Appl Catal A-Gen 2009, 364, 57–64.
[44] Perego C, Villa P. Catalyst preparation methods. Catal Today 1997, 34, 281–305.

[45] Zahmakiran M, Ozkar S. Metal nanoparticles in liquid phase catalysis; from recent advances to future goals. Nanoscale 2011, 3, 3462–3481.
[46] Tsuji Y, Fujihara T. Homogeneous nanosize palladium catalysts. Inorganic Chemistry 2007, 46, 1895–1902.
[47] Astruc D. Palladium nanoparticles as efficient green homogeneous and heterogeneous carbon-carbon coupling precatalysts: A unifying view. Inorganic Chemistry 2007, 46, 1884–1894.
[48] Creamer NJ, Mikheenko IP, Yong P, *et al.* Novel supported Pd hydrogenation bionanocatalyst for hybrid homogeneous/heterogeneous catalysis. Catal Today 2007, 128, 80–87.
[49] Deplanche K, Snape TJ, Hazrati S, Harrad S, Macaskie LE. Versatility of a new bioinorganic catalyst: Palladized cells of Desulfovibrio desulfuricans and application to dehalogenation of flame retardant materials. Environmental Technology 2009, 30, 681–692.
[50] Bennett JA, Attard GA, Deplanche K, *et al.* Improving Selectivity in 2-Butyne-1,4-diol Hydrogenation using Biogenic Pt Catalysts. Acs Catalysis 2012, 2, 504–511.
[51] Depanche K, Bennett JA, Mikheenko IP, *et al.* Catalytic activity of biomass-supported Pd nanoparticles: Influence of the biological component in catalytic efficacy and potential application in 'green' synthesis of fine chemicals and pharmaceuticals. Applied Catalysis B-Environmental 2014, 147, 651–665.
[52] Attard GA, Bennett JA, Mikheenko I, *et al.* Semi-hydrogenation of alkynes at single crystal, nanoparticle and biogenic nanoparticle surfaces: the role of defects in Lindlar-type catalysts and the origin of their selectivity. Faraday Discussions 2013, 162, 57–75.
[53] Wood J, Bodenes L, Bennett J, Deplanche K, Macaskie LE. Hydrogenation of 2-Butyne-1,4-diol Using Novel Bio-Palladium Catalysts. Ind Eng Chem Res 2010, 49, 980–988.
[54] Bennett JA, Creamer NJ, Deplanche K, Macaskie LE, Shannon IJ, Wood J. Palladium supported on bacterial biomass as a novel heterogeneous catalyst: A comparison of Pd/Al2O3 and bio-Pd in the hydrogenation of 2-pentyne. Chem Eng Sci 2010, 65, 282–290.
[55] Crespo-Quesada M, Yarulin A, Jin MS, Xia YN, Kiwi-Minsker L. Structure Sensitivity of Alkynol Hydrogenation on Shape- and Size-Controlled Palladium Nanocrystals: Which Sites Are Most Active and Selective? Journal of the American Chemical Society 2011, 133, 12787–12794.
[56] Schmidt E, Vargas A, Mallat T, Baiker A. Shape-Selective Enantioselective Hydrogenation on Pt Nanoparticles. Journal of the American Chemical Society 2009, 131, 12358–12367.
[57] Kreutzer MT, Kapteijn F, Moulijn JA, Heiszwolf JJ. Multiphase monolith reactors: Chemical reaction engineering of segmented flow in microchannels. Chem Eng Sci 2005, 60, 5895– 5916.
[58] Hutchings GJ, Carrettin S, Landon P, *et al.* New approaches to designing selective oxidation catalysts: Au/C a versatile catalyst. Topics in Catalysis 2006, 38, 223–230.
[59] Haruta M, Kobayashi T, Sano H, Yamada N. Novel gold catalysts for the oxidation of carbon-monoxide at a temperature far below 0-degrees-C. Chemistry Letters 1987, 405–408.
[60] Hutchings GJ, Grady DT. Hydrochlorination of acetylene – the effect of mercuric-chloride concentration on catalyst life. Applied Catalysis 1985, 17, 155–160.
[61] Nkosi B, Coville NJ, Hutchings GJ, Adams MD, Friedl J, Wagner FE. Hydrochlorination of acetylene using gold catalysts - a study of catalyst deactivation. J Catal 1991, 128, 366–377.
[62] Mallat T, Baiker A. Oxidation of alcohols with molecular-oxygen on platinum metal-catalysts in aqueous-solutions. Catal Today 1994, 19, 247–283.
[63] Kluytmans JHJ, Markusse AP, Kuster BFM, Marin GB, Schouten JC. Engineering aspects of the aqueous noble metal catalysed alcohol oxidation. Catal Today 2000, 57, 143–155.
[64] Keresszegi C, Grunwaldt JD, Mallat T, Baiker A. In situ EXAFS study on the oxidation state of Pd/Al2O3 and Bi-Pd/Al2O3 during the liquid-phase oxidation of 1-phenylethanol. J Catal 2004, 222, 268–280.
[65] Gallezot P. Selective oxidation with air on metal catalysts. Catal Today 1997, 37, 405–418.
[66] Venema FR, Peters JA, Vanbekkum H. Platinum-catalyzed oxidation of aldopentoses to aldaric acids. Journal of Molecular Catalysis 1992, 77, 75–85.
[67] Pinxt H, Kuster BFM, Marin GB. Promoter effects in the Pt-catalysed oxidation of propylene glycol. Appl Catal A-Gen 2000, 191, 45–54.
[68] Schuurman Y, Kuster BFM, Vanderwiele K, Marin GB. Selective oxidation of methyl alpha-d-glucoside on carbon supported platinum .3. Catalyst deactivation. Appl Catal A-Gen 1992, 89, 47–68.
[69] Mallat T, Bodnar Z, Baiker A. Promotion and deactivation of platinum catalysts in liquid-phase oxidation of secondary alcohols. Acs Symposium Series 1993, 523, 308–317.
[70] Mallat T, Bodnar Z, Hug P, Baiker A. Selective oxidation of cinnamyl alcohol to cinnamalde-hyde with air over Bi-Pt/alumina catalysts. J Catal 1995, 153, 131–143.
[71] Mori K, Yamaguchi K, Hara T, Mizugaki T, Ebitani K, Kaneda K. Controlled synthesis of hydroxyapatite-supported palladium complexes as highly efficient heterogeneous catalysts. Journal of the American Chemical Society 2002, 124, 11572–11573.
[72] Anderson R, Griffin K, Johnston P, Alsters PL. Selective oxidation of alcohols to carbonyl compounds and carboxylic acids with platinum group metal catalysts. Advanced Synthesis & Catalysis 2003, 345, 517–523.
[73] Mounzer HN, Wood J, Stitt EH. Heterogeneous oxidation of 2-octanol on 5 wt % Pt-1 wt % Bi/Carbon catalyst. Chem Eng Sci 2010, 65, 179–185.
[74] Shaikh A, Al-Dahhan M. Scale-up of Bubble Column Reactors: A Review of Current State-of-the-Art. Ind Eng Chem Res 2013, 52, 8091–8108.
[75] Dudukovic MP, Devanathan N, Holub R. Multiphase reactors – models and experimental-verification. Revue De L Institut Francais Du Petrole 1991, 46, 439 ff.
[76] Degaleesan S, Dudukovic M, Pan Y. Experimental study of gas-induced liquid-flow structures in bubble columns. Aiche Journal 2001, 47, 1913–1931.
[77] Jakobsen HA, Lindborg H, Dorao CA. Modeling of bubble column reactors: Progress and limitations. Ind Eng Chem Res 2005, 44, 5107–5151.

[78] Gupta A, Roy S. Euler-Euler simulation of bubbly flow in a rectangular bubble column: Experimental validation with Radioactive Particle Tracking. Chemical Engineering Journal 2013, 225, 818–836.
[79] Dudukovic MP, Larachi F, Mills PL. Multiphase reactors – revisited. Chem Eng Sci 1999, 54, 1975–1995.
[80] Boyes AP, Chugtai A, Khan Z, Raymahasay S, Sulidis AT, Winterbottom JM. The cocurrent downflow contactor (CDC) as a fixed-bed and slurry reactor for catalytic-hydrogenation. Journal of Chemical Technology and Biotechnology 1995, 64, 55–65.
[81] Boyes AP, Lu XX, Raymahasay S, Saremento S, Tilston MW, Winterbottom JM. The cocurrent downflow contactor (CDC) - mass-transfer and reaction characteristics in unpacked and packed-bed operation. Chemical Engineering Research & Design 1991, 69, 200–202.
[82] Winterbottom JM, Khan Z, Boyes AP, Raymahasay S. Photocatalyzed oxidation of phenol in water using a cocurrent downflow contactor reactor (CDCR). Environmental Progress 1997, 16, 125–131.
[83] Ochuma IJ, Fishwick RP, Wood J, Winterbottom JM. Optimisation of degradation conditions of 1,8-diazabicyclo 5.4.0 undec-7-ene in water and reaction kinetics analysis using a cocurrent downflow contactor photocatalytic reactor. Applied Catalysis B-Environmental 2007, 73, 259– 268.
[84] Ochuma IJ, Fishwick RP, Wood J, Winterbottoom JM. Photocatalytic oxidation of 2,4,6-tri-chlorophenol in water using a cocurrent downflow contactor reactor (CDCR). Journal of Hazardous Materials 2007, 144, 627–633.
[85] Ochuma IJ, Osibo OO, Fishwick RP, *et al*. Three-phase photocatalysis using suspended titania and titania supported on a reticulated foam monolith for water purification. Catal Today 2007, 128, 100–107.
[86] Al-Dahhan MH, Khadilkar MR, Wu Y, Dudukovic MP. Prediction of pressure drop and liquid holdup in high-pressure trickle-bed reactors. Ind Eng Chem Res 1998, 37, 793–798.
[87] Handbook of petroleum refining processes. McGraw-Hill, 2004. at http://site.ebrary.com/id/10180024.)
[88] Vergel C, Euzen JP, Trambouze P, Wauquier JP. 2-phase flow catalytic reactor, influence of hydrodynamics on selectivity. Chem Eng Sci 1995, 50, 3303–3312.
[89] Herrmann U, Emig G. Liquid phase hydrogenation of maleic anhydride and intermediates on copper-based and noble metal catalysts. Ind Eng Chem Res 1997, 36, 2885–2896.
[90] McManus RL, Funk GA, Harold MP, Ng KM. Experimental-study of reaction in trickle-bed reactors with liquid maldistribution. Ind Eng Chem Res 1993, 32, 570–574.
[91] Fortuny A, Font J, Fabregat A. Wet air oxidation of phenol using active carbon as catalyst. Applied Catalysis B-Environmental 1998, 19, 165–173.
[92] Maiti RN, Sen PK, Nigam KDP. Trickle-bed reactors: Liquid distribution and flow texture. Reviews in Chemical Engineering 2004, 20, 57–109.
[93] Baker D. Simultaneous Flow of Oil and Gas. Oil and Gas J 1954, 53, 183–195.
[94] Al-Naimi SA, Al-Sudani FTJ, Halabia EK. Hydrodynamics and flow regime transition study of trickle bed reactor at elevated temperature and pressure. Chemical Engineering Research & Design 2011, 89, 930–939.
[95] Burghardt A, Bartelmus G, Janecki D, Szlemp A. Hydrodynamics of a three-phase fixed-bed reactor operating in the pulsing flow regime at an elevated pressure. Chem Eng Sci 2002, 57, 4855–4863.
[96] Anadon LD, Sederman AJ, Gladden LF. Mechanism of the trickle-to-pulse flow transition in fixed-bed reactors. Aiche Journal 2006, 52, 1522–1532.
[97] Gladden LF, Anadon LD, Dunckley CP, Mantle MD, Sederman AJ. Insights into gas-liquid-solid reactors obtained by magnetic resonance imaging. Chem Eng Sci 2007, 62, 6969–6977.
[98] Gladden LF, Anadon LD, Lim MHM, Sederman AJ, Stitt EH. Insights into the mechanism of the trickle-to-pulse transition in trickle-bed reactors. Ind Eng Chem Res 2005, 44, 6320–6331.
[99] Anadon LD, Sederman AJ, Gladden LF. Rationalising MRI, conductance and pressure drop measurements of the trickle-to-pulse transition in trickle beds. Chem Eng Sci 2008, 63, 4640–4648.
[100] Sederman AJ, Mantle MD, Dunckley CP, Huang ZY, Gladden LF. In situ MRI study of 1-octene isomerisation and hydrogenation within a trickle-bed reactor. Catalysis Letters 2005, 103, 1–8.
[101] Kulkarni RR, Wood J, Winterbottom JM, Stitt EH. Effect of fines and porous catalyst on hydrodynamics of trickle bed reactors. Ind Eng Chem Res 2005, 44, 9497–9501.
[102] Iliuta I, Thyrion FC, Muntean O. Residence time distribution of the liquid in two-phase cocurrent downflow in packed beds: Air/Newtonian and non-Newtonian liquid systems. Can J Chem Eng 1996, 74, 783–796.
[103] Iliuta I, Larachi F, Al-Dahhan MH. Multiple-zone model for partially wetted trickle flow hydrodynamics. Chemical Engineering Research & Design 2000, 78, 982–990.
[104] Khadilkar MR, Mills PL, Dudukovic MP. Trickle-bed reactor models for systems with a volatile liquid phase. Chem Eng Sci 1999, 54, 2421–2431.
[105] Ostrovskii NM, J. W. Reaction and Capillary Condensation in Dispersed Porous Particles. Surfactant science series 2006, 130, 601–640.
[106] Wood J, Gladden LF. Modelling diffusion and reaction accompanied by capillary condensation using three-dimensional pore networks. Part 1. Fickian diffusion and pseudo-first-order reaction kinetics. Chem Eng Sci 2002, 57, 3033–3045.
[107] Wood J, Gladden LF, Keil FJ. Modelling diffusion and reaction accompanied by capillary condensation using three-dimensional pore networks. Part 2. Dusty gas model and general reaction kinetics. Chem Eng Sci 2002, 57, 3047–3059.
[108] Wang YN, Chen JW, Larachi F. Modelling and simulation of trickle-bed reactors using computational fluid dynamics: A state-of-the-art review. Can J Chem Eng 2013, 91, 136–180.
[109] Hickman DA, Holbrook MT, Mistretta S, Rozeveld SJ. Successful Scale-up of an Industrial Trickle Bed Hydrogenation Using Laboratory Reactor Data. Ind Eng Chem Res 2013, 52, 15287–15292.
[110] De Vos DE, Jacobs PA. Heterogenization of Mn and Fe complex oxidation catalysts. Catal Today 2000, 57, 105–114.
[111] Augustine RL, Tanielyan SK, Mahata N, Gao Y, Zsigmond A, Yang H. Anchored homogeneous catalysts: the role of the heteropoly acid anchoring agent. Appl Catal A-Gen 2003, 256, 69– 76.

[112] Augustine RL, Goel P, Mahata N, Reyes C, Tanielyan SK. Anchored homogeneous catalysts: high turnover number applications. Journal of Molecular Catalysis a-Chemical 2004, 216, 189–197.
[113] Young JF, Osborn JA, Jardine FH, Wilkinso.G. Hydride intermediates in homogeneous hydrogenation reactions of olefins and acetylenes using rhodium catalysts. Chemical Communications 1965, 131 ff.
[114] Vries JGdE, Cornelis J. The handbook of homogeneous hydrogenation. Weinheim; [Great Britain], Wiley-VCH, 2007.
[115] Baiker A. Progress in asymmetric heterogeneous catalysis: Design of novel chirally modified platinum metal catalysts. Journal of Molecular Catalysis a-Chemical 1997, 115, 473–493.
[116] Toukoniitty E, Maki-Arvela P, Neyestanaki AK, Salmi T, Murzin DY. Continuous hydrogenation of 1-phenyl-1,2-propanedione under transient and steady-state conditions: regioselectivity, enantio selectivity and catalyst deactivation. Appl Catal A-Gen 2002, 235, 125–138.
[117] Kunzle N, Soler JW, Baiker A. Continuous enantioselective hydrogenation in fixed-bed reactor: towards process intensification. Catal Today 2003, 79, 503–509.
[118] Kunzle N, Soler JW, Mallat T, Baiker A. Enantioselective hydrogenation on palladium – Limitations of continuous fixed-bed reactor operation. J Catal 2002, 210, 466–470.
[119] Al Herz MA, Tsoligkas AN, Simmons MJH, Wood J. Enantioselective hydrogenation of dimethyl itaconate with immobilised rhodium-duphos complex in a recirculating fixed-bed reactor. Appl Catal A-Gen 2011, 396, 148–158.
[120] Osborn JA, Jardine FH, Young JF, Wilkinson G. The preparation and properties of tris(triphenyl-phosphine)halogenorhodium(I) and some reactions thereof including catalytic homogeneous hydrogenation of olefins and acetylenes and their derivatives. Journal of the Chemical Society A: Inorganic, Physical, Theoretical 1966, 1711–1732.
[121] Shah A, Fishwick R, Wood J, Leeke G, Rigby S, Greaves M. A review of novel techniques for heavy oil and bitumen extraction and upgrading. Energy & Environmental Science 2010, 3, 700–714.
[122] Shah A, Fishwick RP, Leeke GA, Wood J, Rigby SP, Greaves M. Experimental Optimization of Catalytic Process In Situ for Heavy-Oil and Bitumen Upgrading. Journal of Canadian Petroleum Technology 2011, 50, 33–47.
[123] Hart A, Shah A, Leeke G, Greaves M, Wood J. Optimization of the CAPRI Process for Heavy Oil Upgrading: Effect of Hydrogen and Guard Bed. Ind Eng Chem Res 2013, 52, 15394–15406.
[124] Christian, Mitchell M, Kenis PJA. Ceramic microreactors for on-site hydrogen production from high temperature steam reforming of propane. Lab on a Chip 2006, 6, 1328–1337.
[125] Ruettinger W, Ilinich O, Farrauto RJ. A new generation of water gas shift catalysts for fuel cell applications. Journal of Power Sources 2003, 118, 61–65.
[126] Brooks KP, Hu J, Zhu H, Kee RJ. Methanation of carbon dioxide by hydrogen reduction using the Sabatier process in microchannel reactors. Chem Eng Sci 2007, 62, 1161–1170.
[127] Guettel R, Kunz U, Turek T. Reactors for Fischer-Tropsch synthesis. Chem Eng Technol 2008, 31, 746–754.
[128] Sung M, Kato S, Kawanami F, Sudo M. Evaluation of an air-cleaning unit having photocatalytic sheets to remove acetaldehyde from indoor air. Building and Environment 2010, 45, 2002– 2007.
[129] Van Gerven T, Mul G, Moulijn J, Stankiewicz A. A review of intensification of photocatalytic processes. Chemical Engineering and Processing 2007, 46, 781–789.
[130] Lisi L, Pirone R, Russo G, Stanzione V. Cu-ZSM5 based monolith reactors for NO decomposition. Chemical Engineering Journal 2009, 154, 341–347.
[131] Dhanushkodi SR, Mahinpey N, Wilson M. Kinetic and 2D reactor modeling for simulation of the catalytic reduction of NOx in the monolith honeycomb reactor. Process Safety and Environmental Protection 2008, 86, 303–309.
[132] Cybulski A, Stankiewicz A, Albers RKE, Moulijn JA. Monolithic reactors for fine chemicals industries: A comparative analysis of a monolithic reactor and a mechanically agitated slurry reactor. Chem Eng Sci 1999, 54, 2351–2358.
[133] Kreutzer MT, Du P, Heiszwolf JJ, Kapteijn F, Moulijn JA. Mass transfer characteristics of three-phase monolith reactors. Chem Eng Sci 2001, 56, 6015–6023.
[134] Tsoligkas AN, Simmons MJH, Wood J, Frost CG. Kinetic and selectivity studies of gas-liquid reaction under Taylor flow in a circular capillary. Catal Today 2007, 128, 36–46.
[135] Tsoligkas AN, Simmons MJH, Wood J. Two phase gas-liquid reaction studies in a circular capillary. Chem Eng Sci 2007, 62, 5397–5401.
[136] Mogalicherla AK, Kunzru D. Performance of monolithic reactors in film flow. Chemical Engineering Research & Design 2010, 88, 1057–1066.
[137] Nijhuis TA, Kreutzer MT, Romijn ACJ, Kapteijn F, Moulijn JA. Monolithic catalysts as more efficient three-phase reactors. Catal Today 2001, 66, 157–165.
[138] Enache DI, Landon P, Lok CM, Pollington SD, Stitt EH. Direct comparison of a trickle bed and a monolith for hydrogenation of pyrolysis gasoline. Ind Eng Chem Res 2005, 44, 9431–949.
[139] Pollington SD, Enache DI, Landon P, *et al.* Enhanced selective glycerol oxidation in multiphase structured reactors. Catal Today 2009, 145, 169–175.
[140] Patrick TA, Abraham MA. Evaluation of a monolith-supported Pt/Al2O3 catalyst for wet oxidation of carbohydrate-containing waste streams. Environmental Science & Technology 2000, 34, 3480–3488.
[141] Rodrigues CP, da Silva VT, Schmal M. Partial oxidation of ethanol over cobalt oxide based cordierite monolith catalyst. Applied Catalysis B-Environmental 2010, 96, 1–9.
[142] Albers RE, Nystrom M, Siverstrom M, *et al.* Development of a monolith-based process for H2O2-production: from idea to large-scale implementation. Catal Today 2001, 69, 247–252.
[143] Thulasidas TC, Cerro RL, Abraham MA. The monolith froth reactor - residence time modeling and analysis. Chemical Engineering Research & Design 1995, 73, 314–319.
[144] Stutz MJ, Poulikakos D. Optimum washcoat thickness of a monolith reactor for syngas production by partial oxidation of methane. Chem Eng Sci 2008, 63, 1761–1770.

[145] Kreutzer MT, Kapteijn F, Moulijn JA. Shouldn't catalysts shape up? Structured reactors in general and gas-liquid monolith reactors in particular. Catal Today 2006, 111, 111–118.
[146] Satterfield CN, Ozel F. Some characteristics of 2-phase flow in monolithic catalyst structures. Industrial & Engineering Chemistry Fundamentals 1977, 16, 61–67.
[147] Taitel Y, Bornea D, Dukler AE. Modeling flow pattern transitions for steady upward gas-liquid flow in vertical tubes. Aiche Journal 1980, 26, 345–354.
[148] Tsoligkas A, Simmons MJH, Wood J. Influence of orientation upon the hydrodynamics of gas-liquid flow for square channels in monolith supports. Chem Eng Sci 2007, 62, 4365–4378.
[149] Stitt EH, Jackson SD, Shipley DG, King F. Modelling propane dehydrogenation in a rotating monolith reactor. Catal Today 2001, 69, 217–226.
[150] Subramanian R, Panuccio GJ, Krummenacher JJ, Lee IC, Schmidt LD. Catalytic partial oxidation of higher hydrocarbons: reactivities and selectivities of mixtures. Chem Eng Sci 2004, 59, 5501–5507.
[151] Hoelderich WF. Environmentally benign manufacturing of fine and intermediate chemicals. Catal Today 2000, 62, 115–130.
[152] Molga EJ, Westerterp KR. Kinetics of the hydrogenation of 2,4-dinitrotoluene over a palladium on alumina catalyst. Chem Eng Sci 1992, 47, 1733–1749.
[153] Benaissa M, LeRoux GC, Joulia X, Chaudhari RV, Delmas H. Kinetic modeling of the hydrogenation of 1,5,9-cyclododecatriene on Pd/Al2O3 catalyst including isomerization. Ind Eng Chem Res 1996, 35, 2091–2095.